US009188798B2

(12) **United States Patent**
Taylor

(10) **Patent No.: US 9,188,798 B2**
(45) **Date of Patent: Nov. 17, 2015**

(54) **OPTICAL CLOSED LOOP MICRORESONATOR AND THYRISTOR MEMORY DEVICE**

(75) Inventor: **Geoff W. Taylor**, Mansfield, CT (US)

(73) Assignees: **Opel Solar, Inc.**, Storrs Mansfield, CT (US); **The University of Connecticut**, Farmington, CT (US)

(*) Notice: Subject to any disclaimer, the term of this patent is extended or adjusted under 35 U.S.C. 154(b) by 0 days.

(21) Appl. No.: **14/238,649**

(22) PCT Filed: **Aug. 17, 2012**

(86) PCT No.: **PCT/US2012/051265**

§ 371 (c)(1),
(2), (4) Date: **Feb. 12, 2014**

(87) PCT Pub. No.: **WO2013/025964**

PCT Pub. Date: **Feb. 21, 2013**

(65) **Prior Publication Data**

US 2014/0241660 A1 Aug. 28, 2014

Related U.S. Application Data

(60) Provisional application No. 61/525,072, filed on Aug. 18, 2011.

(51) **Int. Cl.**

G02F 1/035	(2006.01)
G02F 1/017	(2006.01)
G02B 6/12	(2006.01)
G02B 6/293	(2006.01)
G02B 6/124	(2006.01)
G02B 6/125	(2006.01)

(Continued)

(52) **U.S. Cl.**
CPC ***G02F 1/01708*** (2013.01); ***G02B 6/124*** (2013.01); ***G02B 6/125*** (2013.01); ***G02B 6/12007*** (2013.01); ***G02B 6/29338*** (2013.01); ***H01L 45/06*** (2013.01); *B82Y 20/00* (2013.01); *G02F 2001/0154* (2013.01); *Y10S 977/755* (2013.01)

(58) **Field of Classification Search**
CPC G02F 1/01708; H01L 45/06; G02B 6/124; G02B 6/125; G02B 6/29338; G02B 6/12007
See application file for complete search history.

(56) **References Cited**

U.S. PATENT DOCUMENTS

5,790,583 A 8/1998 Ho
6,031,243 A 2/2000 Tayor

(Continued)

FOREIGN PATENT DOCUMENTS

WO WO 02/071490 A1 9/2002

OTHER PUBLICATIONS

Design of Micro Resonator Quantum Well Intensity Modulators Based on an Absorption Blue-Shift; Y. Zhang et al., Dept. of ECE, Univ. of Conn., Aug. 2011.

(Continued)

Primary Examiner — Ryan Lepisto
(74) *Attorney, Agent, or Firm* — Gordon & Jacobson P.C.

(57) **ABSTRACT**

A monolithic semiconductor device that includes a waveguide structure optically coupled to an optical resonator. The optical resonator is adapted to process light at a predetermined wavelength. The optical resonator includes a closed loop waveguide having a plurality of straight sections that are optically coupled together by bend sections.

32 Claims, 32 Drawing Sheets

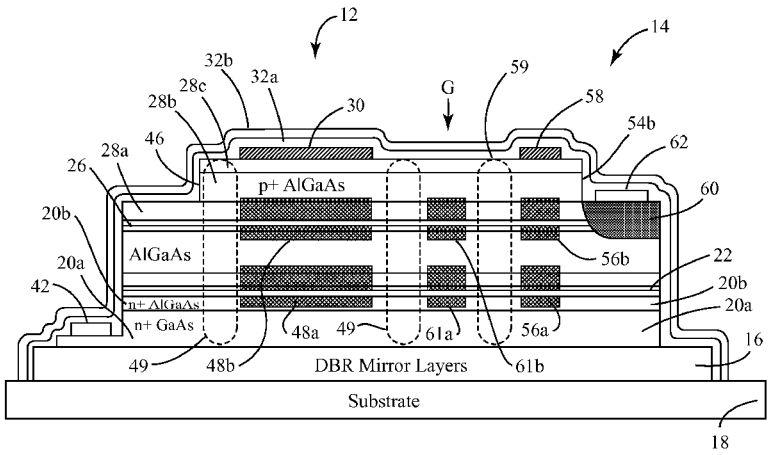

(51) **Int. Cl.**

H01L 45/00	(2006.01)
B82Y 20/00	(2011.01)
G02F 1/015	(2006.01)

(56) **References Cited**

U.S. PATENT DOCUMENTS

6,118,908	A	9/2000	Bischel et al.	
6,275,296	B1 *	8/2001	Numai	356/459
6,479,844	B2	11/2002	Taylor	
6,639,930	B2 *	10/2003	Griffel et al.	372/94
6,841,795	B2	1/2005	Taylor et al.	
6,849,866	B2	2/2005	Taylor	
6,853,014	B2	2/2005	Taylor et al.	
6,865,314	B1	3/2005	Blair et al.	
6,870,207	B2	3/2005	Taylor	
6,873,273	B2	3/2005	Taylor et al.	
6,954,473	B2	10/2005	Dehmubed et al.	
6,995,407	B2	2/2006	Taylor et al.	
7,332,752	B2	2/2008	Taylor et al.	
7,657,132	B1	2/2010	Yap et al.	
7,713,803	B2 *	5/2010	Jin et al.	438/172
7,750,763	B2	7/2010	Prabmayer	
2002/0176087	A1	11/2002	Numai	
2004/0081467	A1 *	4/2004	Taylor et al.	398/161
2004/0188669	A1 *	9/2004	Atanackovic et al.	257/15
2009/0190875	A1	7/2009	Bratkovski et al.	
2009/0239323	A1	9/2009	Tan et al.	

OTHER PUBLICATIONS

Micro-Optical Resonators for Microlasers and Integrated Optoelectronics, Trevor M. Benson et al., George Green Institute for Electromagnetics Research, 2006.

Resonant Optoelectronic Thyristor Switches as Elements for Optical Switching Fabrics, P. C. Pile et al., Dept. of ECE, Univ. of Conn., Aug. 23, 2011.

Planar Comer-Cut Square Microcavities: Ray Optics and FDTD Analysis; Chung Yan Fong et al., Optics Express, Oct. 4, 2004, vol. 12, No. 20.

Transistor Based Quantum Well Optical Modulator and Its Performance in RF Links, Y.Zhang et al., Proc. SPIE 7817, 12-22 (2010).

U.S. Appl. No. 08/949,504, filed Oct. 14, 1997, Geoff W. Taylor.

U.S. Appl. No. 09/710,217, filed Nov. 10, 2000, Geoff W. Taylor.

U.S. Appl. No. 60/376,238, filed Apr. 26, 2002, Geoff W. Taylor.

* cited by examiner

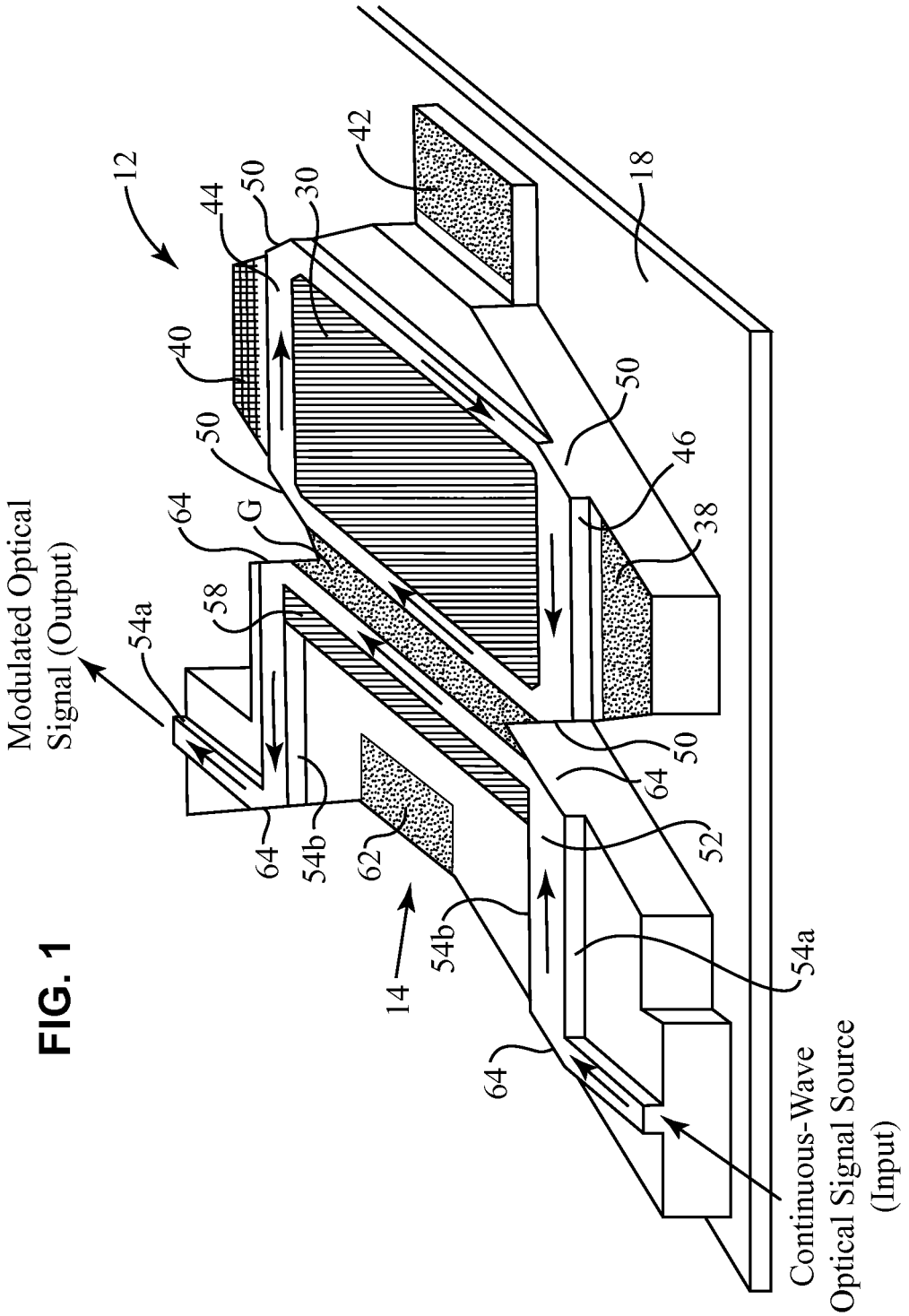
Modulated Optical
Signal (Output)
Continuous-Wave
Optical Signal Source
(Input)
12
14
18
30
38
40
42
44
46
50
52
54a
54b
58
62
64
G

FIG. 1

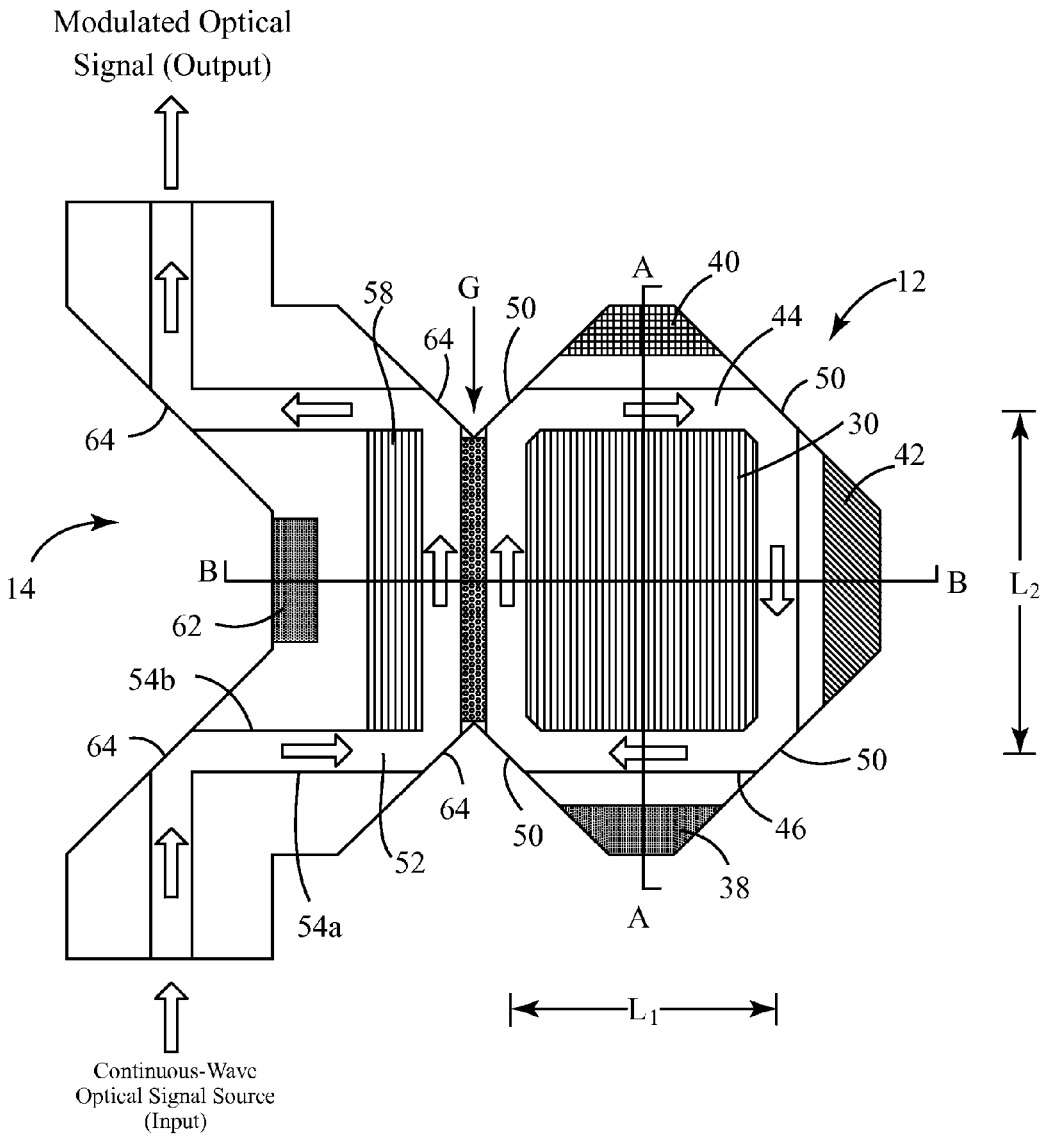
Modulated Optical
Signal (Output)
58
G
64
50
A
40
12
44
50
30
42
64
14
B
B
62
54b
64
50
64
50
46
52
38
54a
A
L_1
L_2
Continuous-Wave
Optical Signal Source
(Input)

FIG. 2

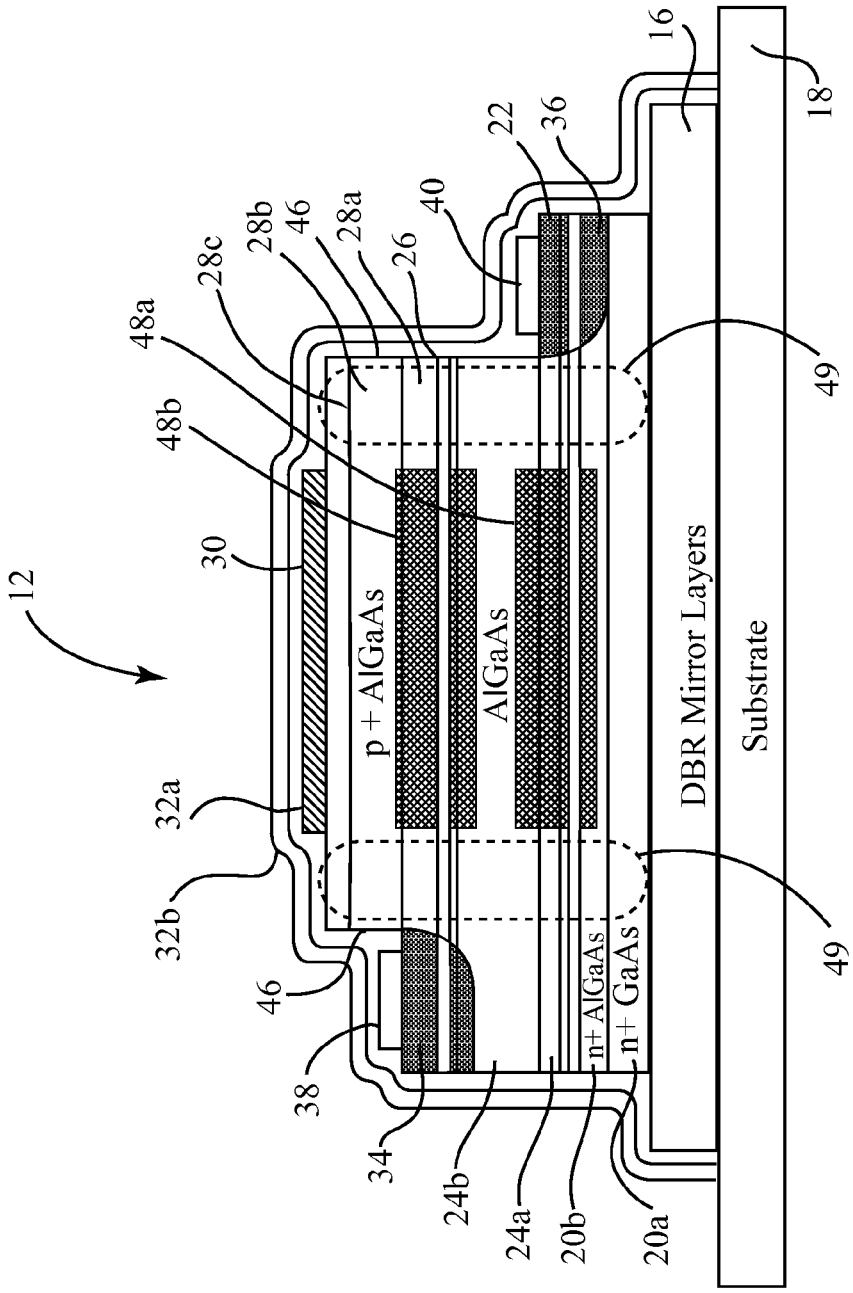
12
30
48a
48b
28c
28b
46
28a
26
40
22
36
16
18
49
49
32a
32b
46
38
34
24b
24a
20b
20a
p + AlGaAs
AlGaAs
n+ AlGaAs
n+ GaAs
DBR Mirror Layers
Substrate

FIG. 3

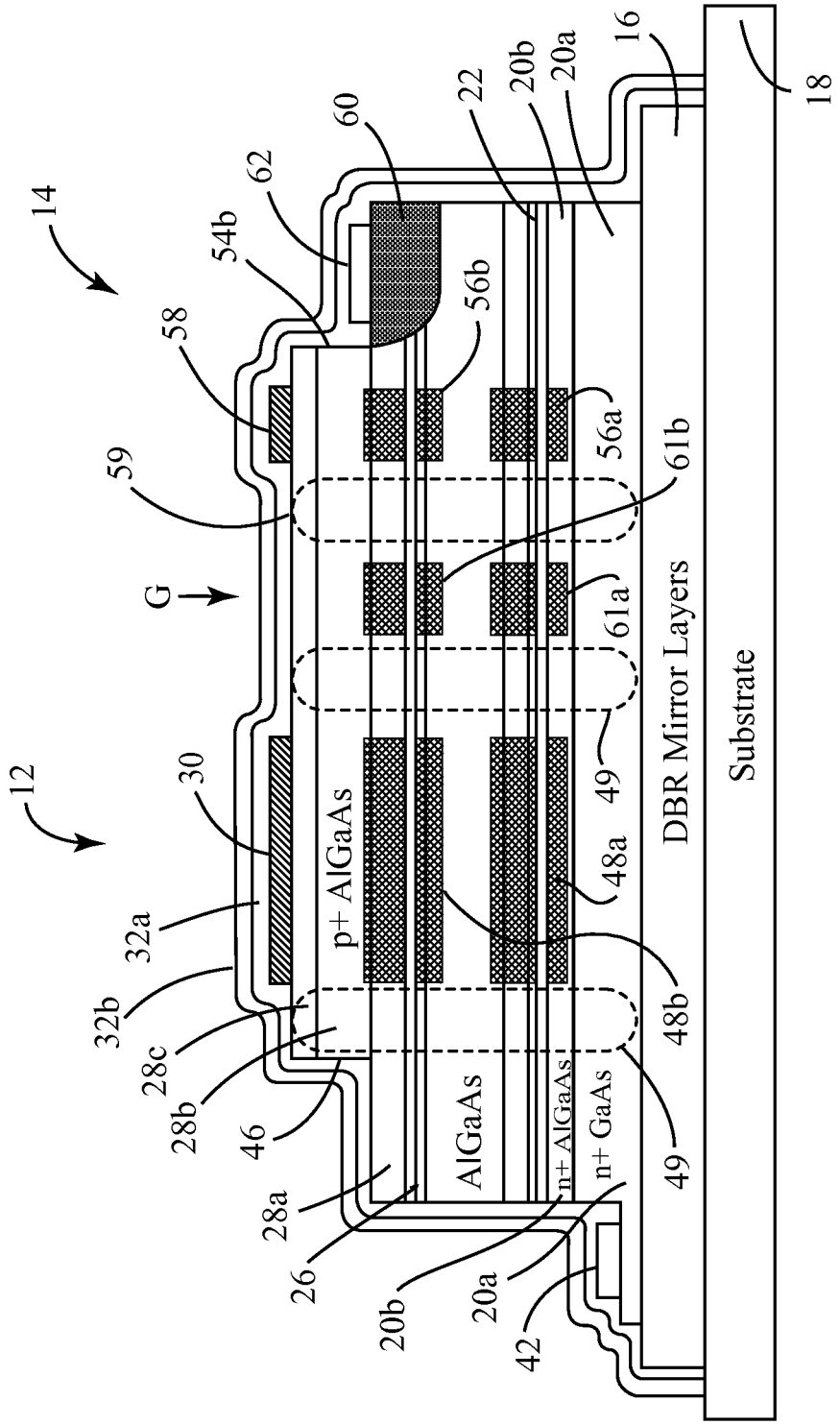
14
12
G
59
58
54b
62
60
56b
22
20b
20a
16
18
56a
61b
61a
49
48a
48b
30
32a
32b
28c
28b
46
28a
26
20b
20a
42
p+ AlGaAs
AlGaAs
n+ AlGaAs
n+ GaAs
DBR Mirror Layers
Substrate

FIG. 4

FIG. 5(A)

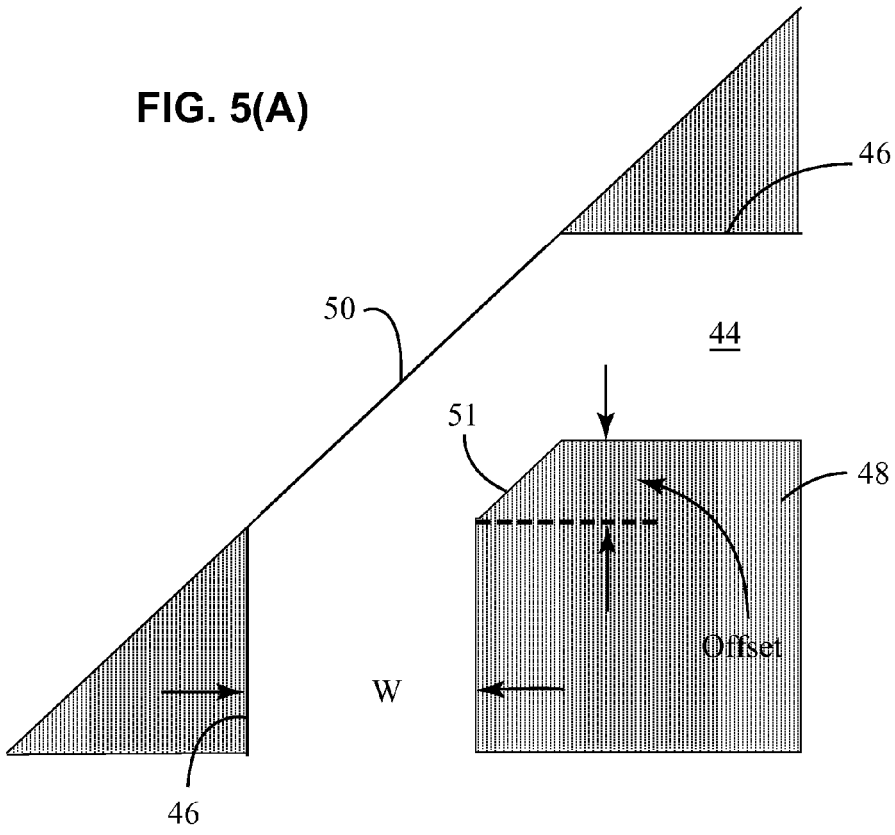

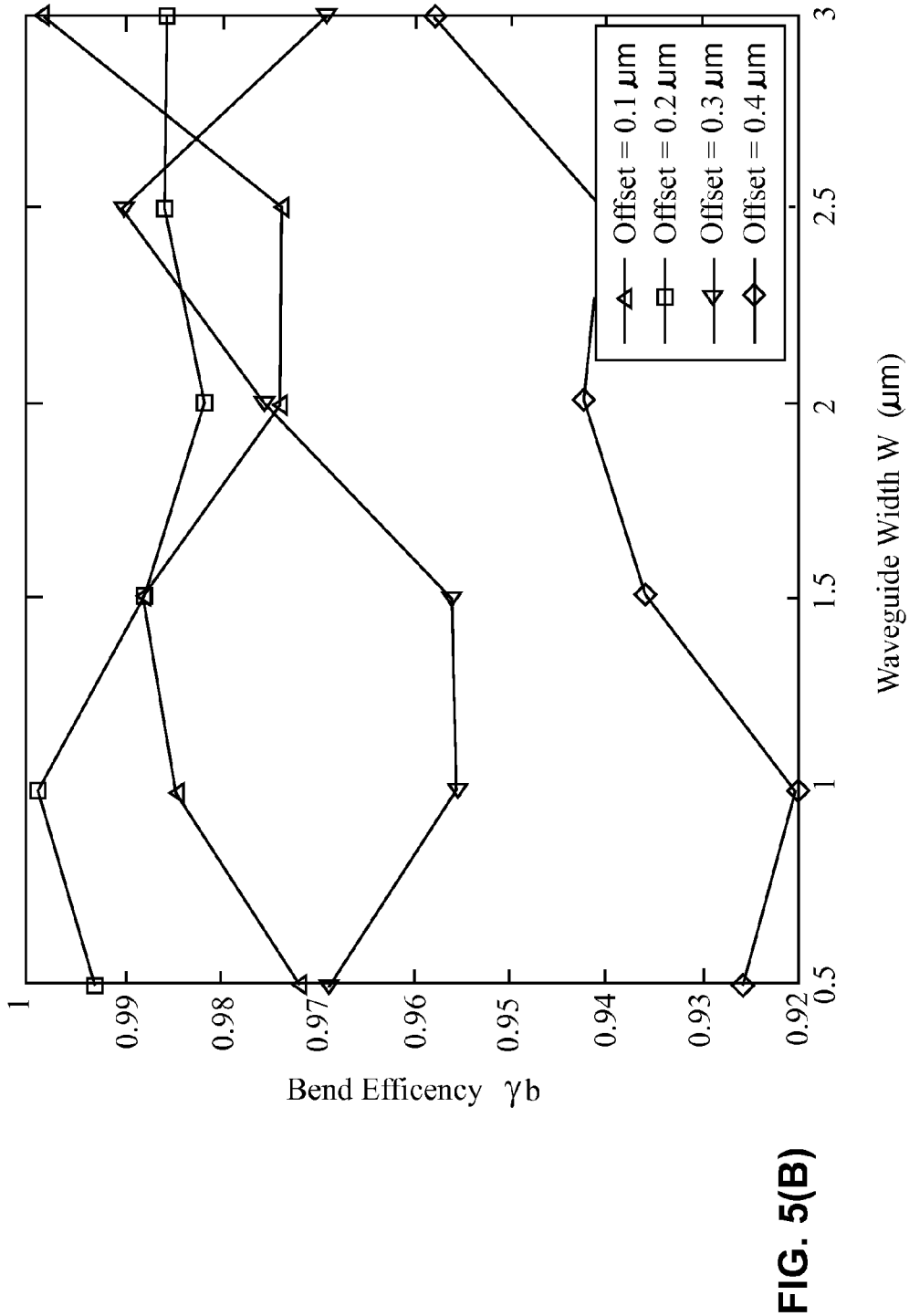
Offset = 0.1 μm
Offset = 0.2 μm
Offset = 0.3 μm
Offset = 0.4 μm
Bend Efficency γb
Waveguide Width W (μm)
1
0.99
0.98
0.97
0.96
0.95
0.94
0.93
0.92
0.5
1
1.5
2
2.5
3

FIG. 5(B)

FIG. 6

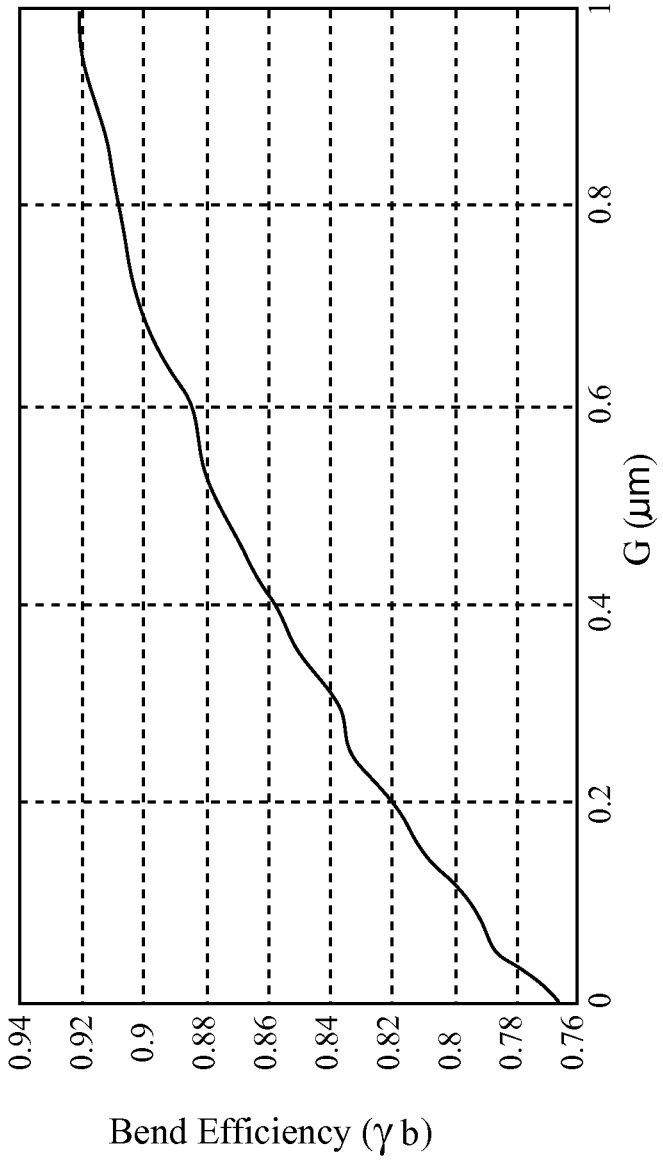
0.94
0.92
0.9
0.88
0.86
0.84
0.82
0.8
0.78
0.76
Bend Efficiency (γ b)
0
0.2
0.4
0.6
0.8
1
G (μm)

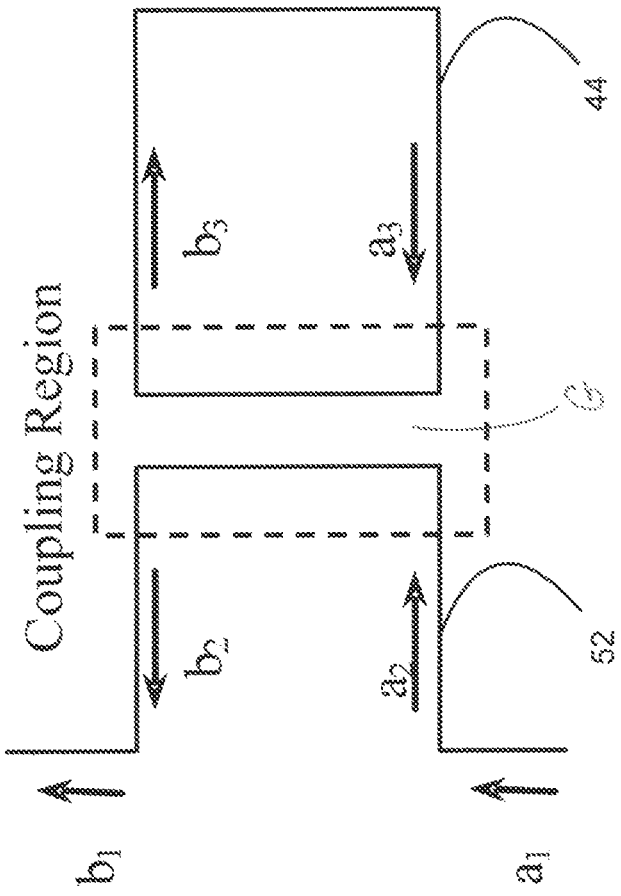

FIG. 7

FIG. 8

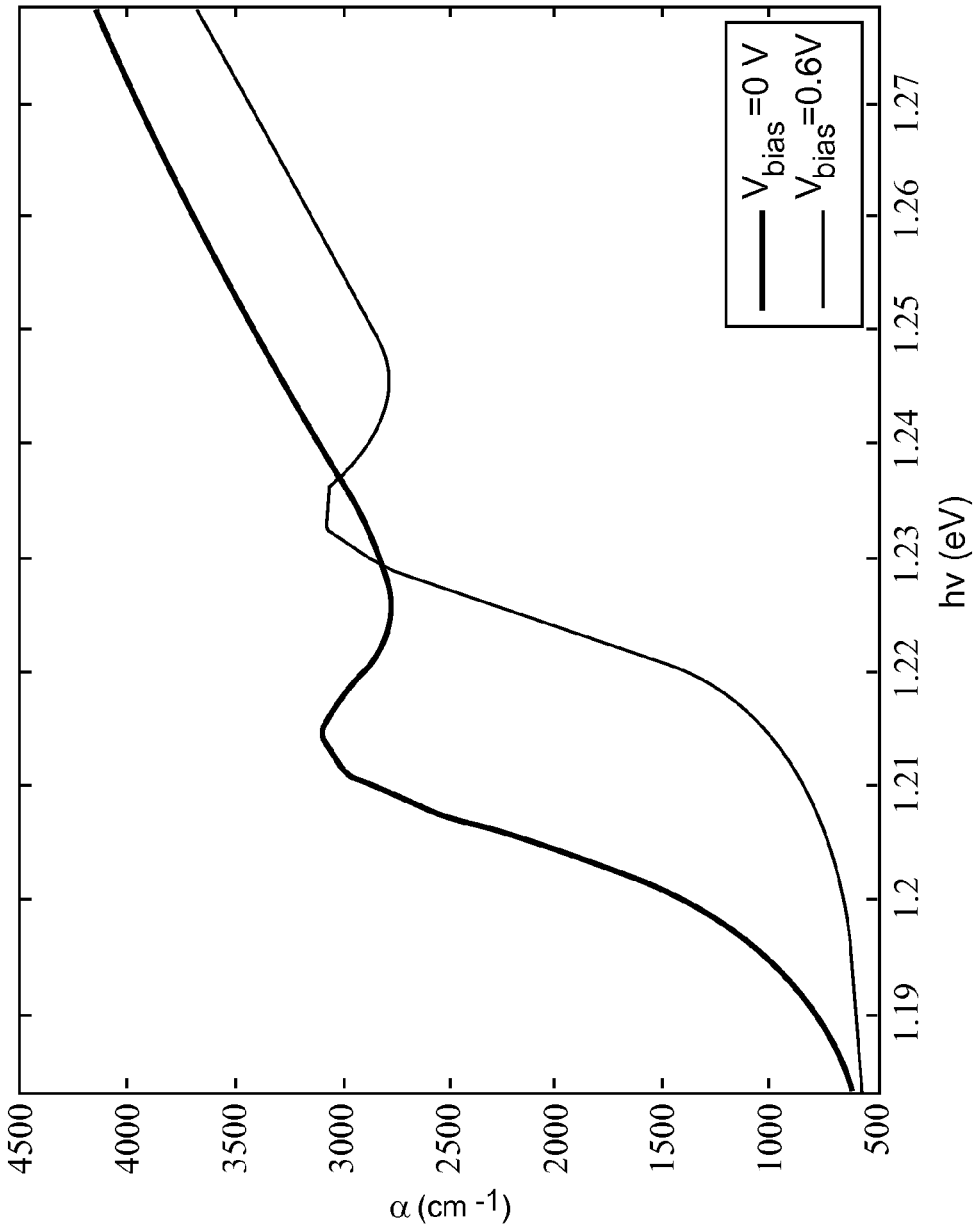
4500
4000
3500
3000
2500
2000
1500
1000
500
α (cm -1)
1.19
1.2
1.21
1.22
1.23
1.24
1.25
1.26
1.27
hv (eV)
V bias =0 V
V bias =0.6V

FIG. 9

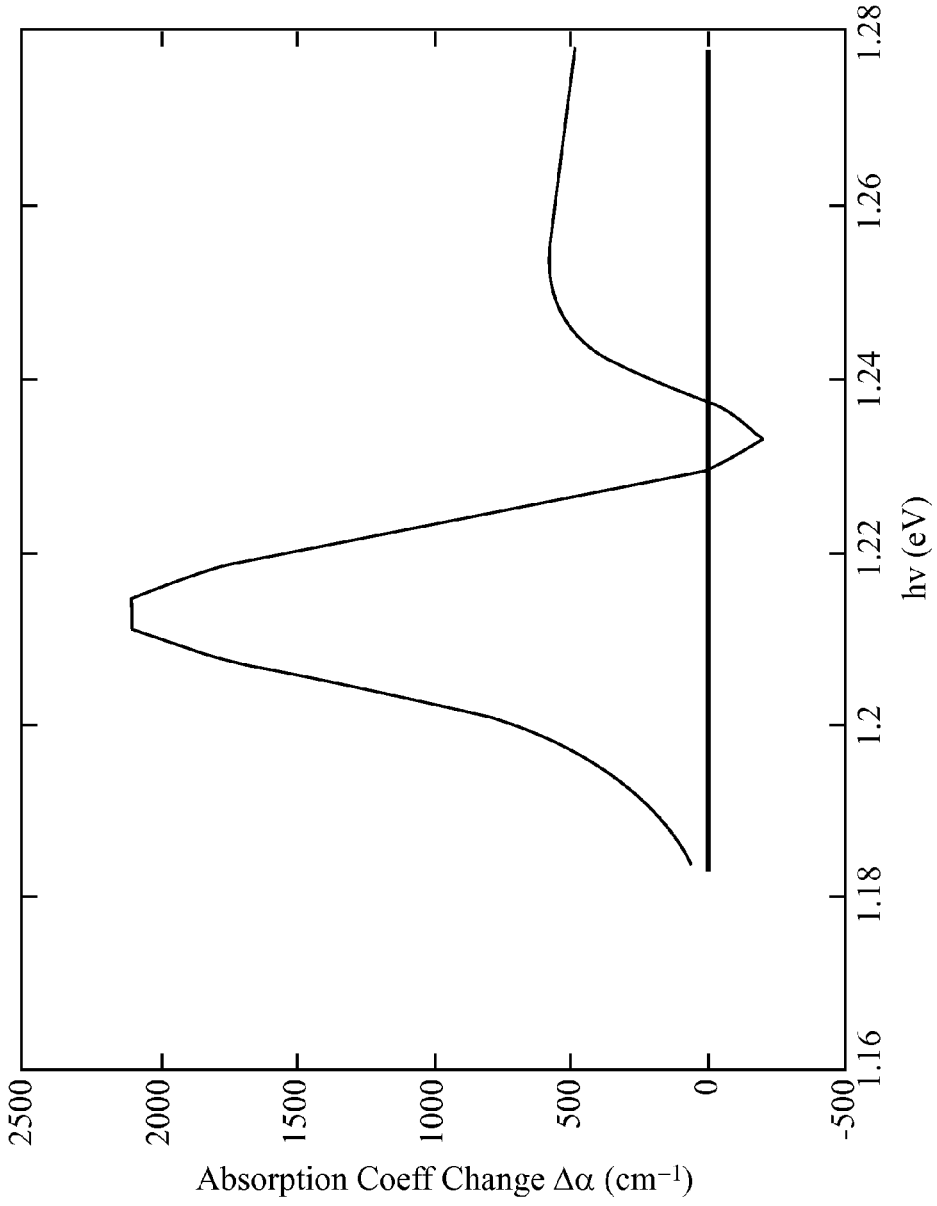
2500
2000
1500
1000
500
0
-500
Absorption Coeff Change Δα (cm⁻¹)
1.16
1.18
1.2
1.22
1.24
1.26
1.28
hv (eV)

FIG. 10

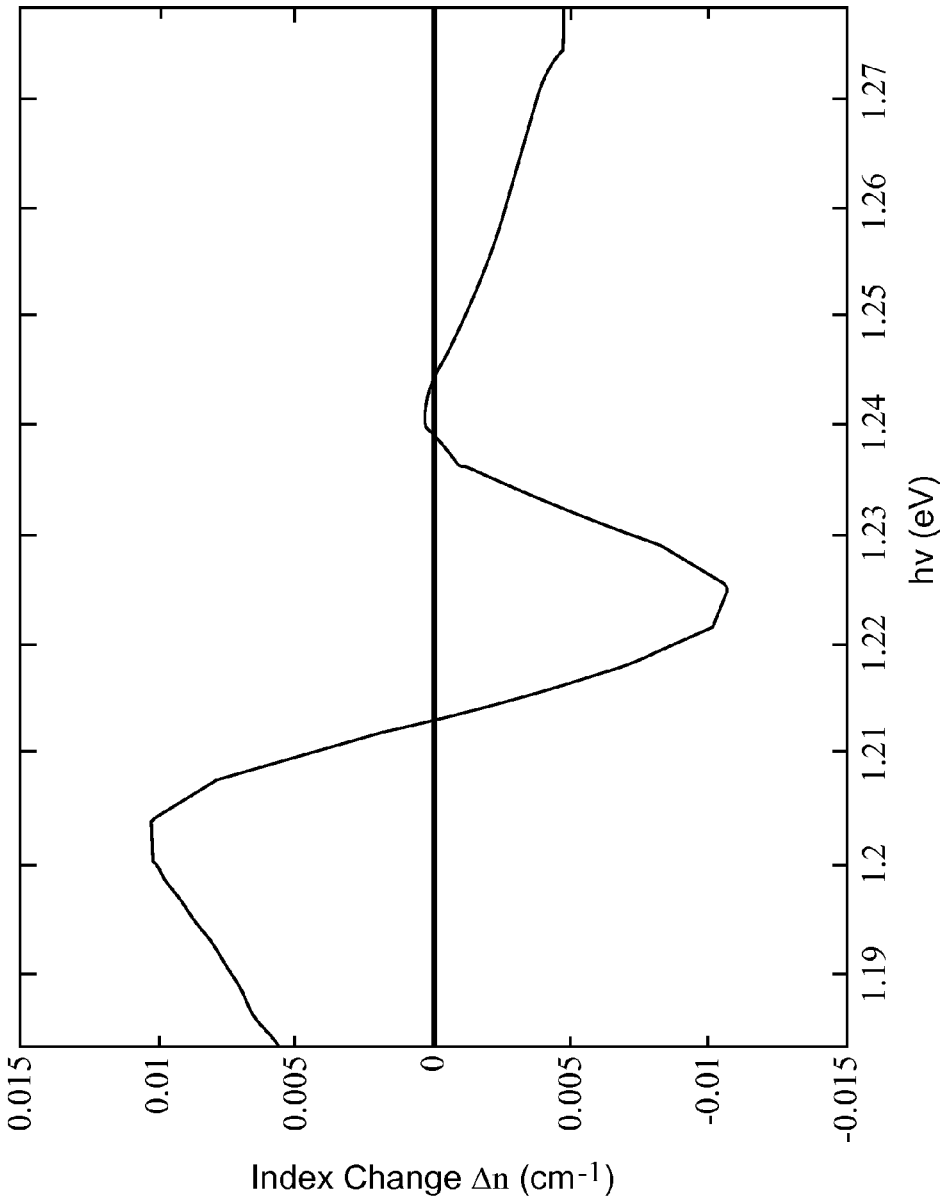
0.015
0.01
0.005
0
0.005
-0.01
-0.015
Index Change Δn (cm-1)
1.19
1.2
1.21
1.22
1.23
1.24
1.25
1.26
1.27
hv (eV)

FIG. 11

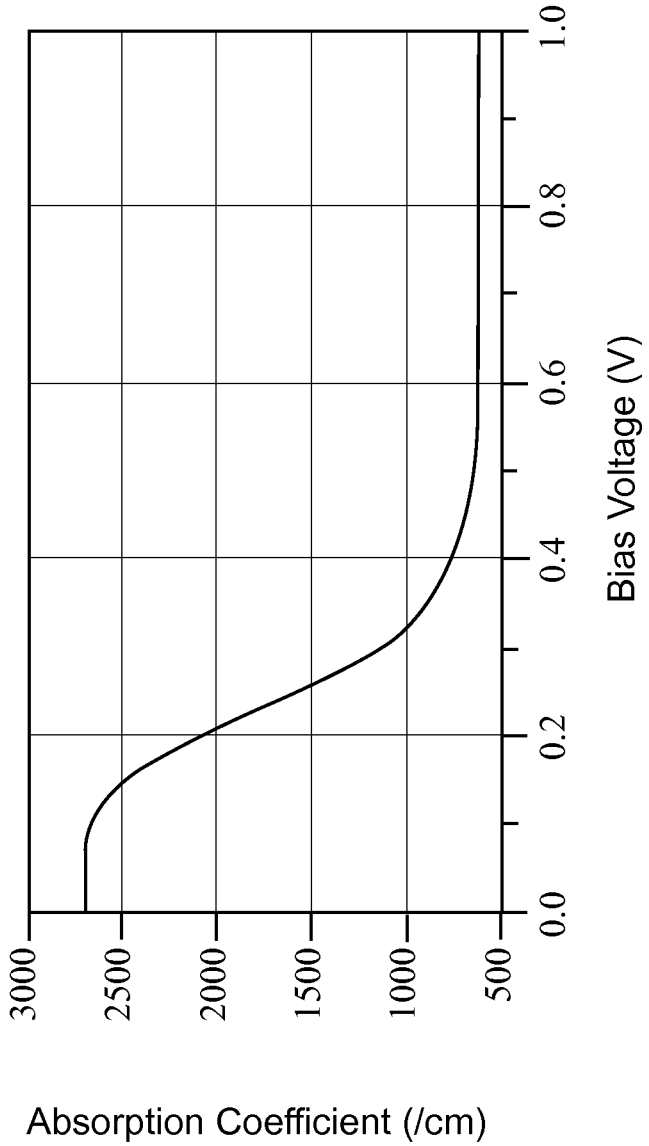
3000
2500
2000
1500
1000
500
0.0
0.2
0.4
0.6
0.8
1.0
Bias Voltage (V)
Absorption Coefficient (/cm)

FIG. 12

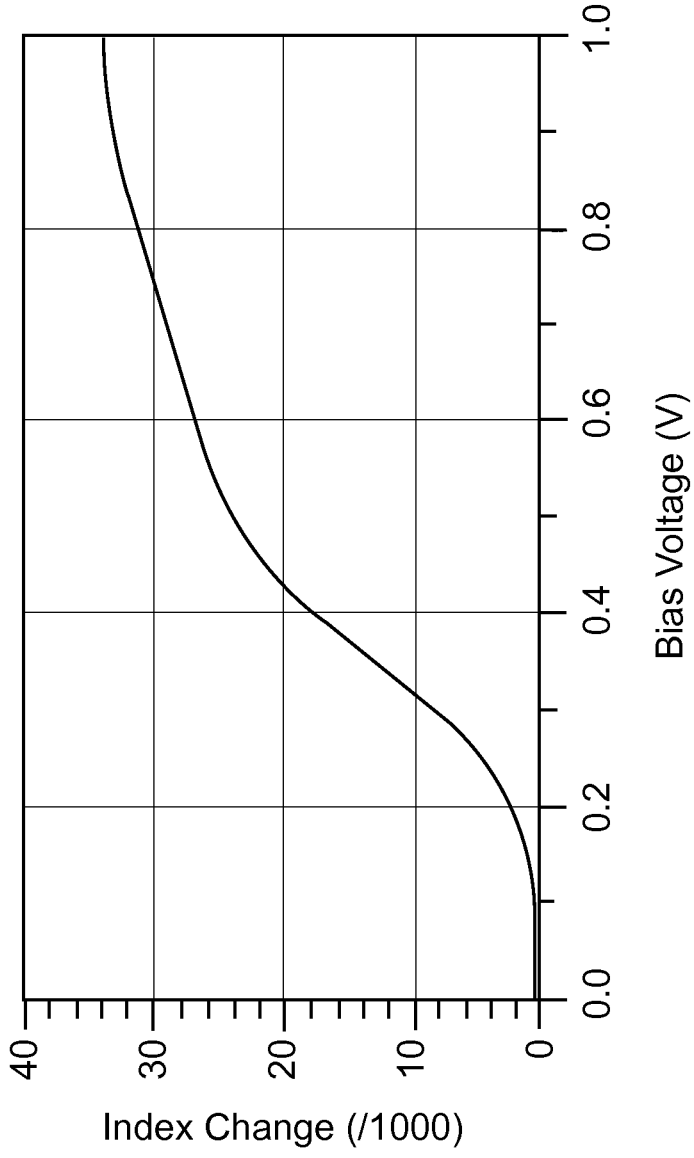

FIG. 13

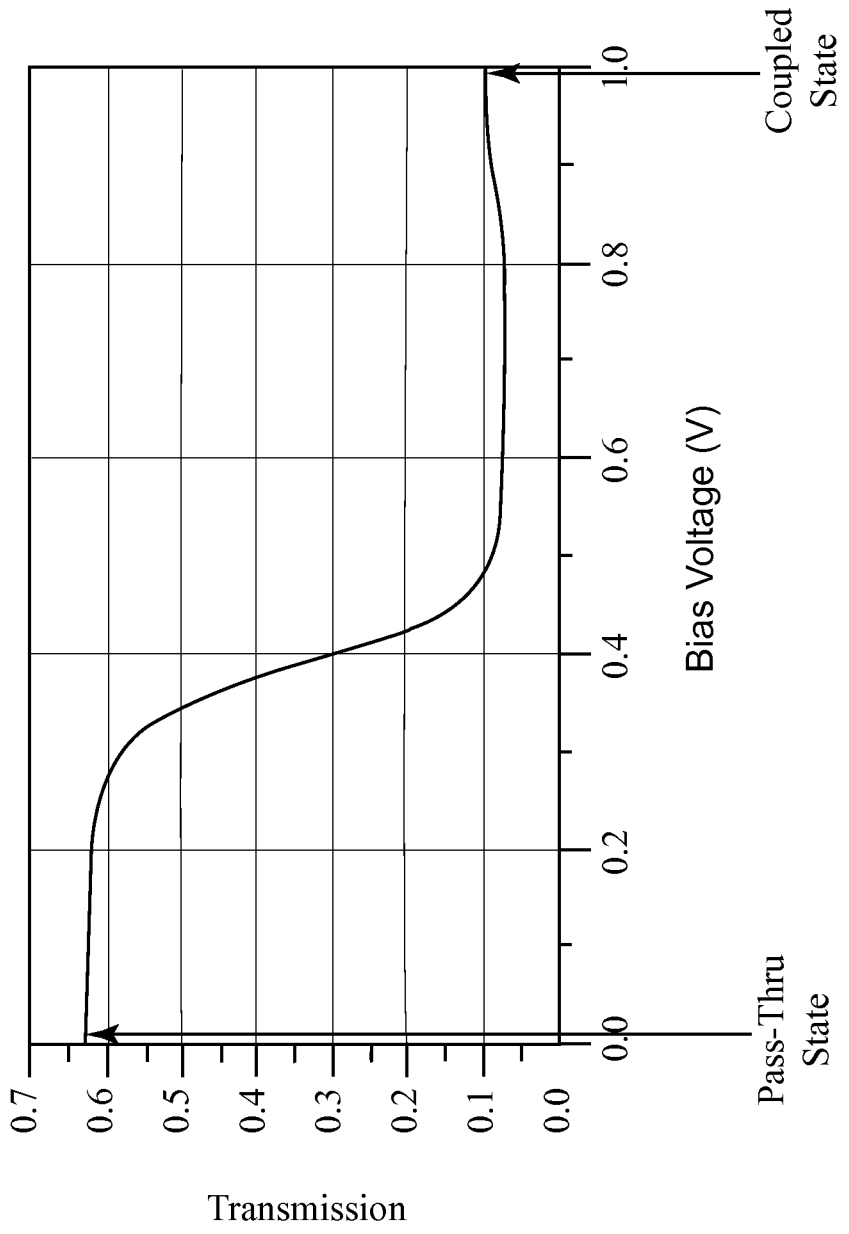
Transmission
0.7
0.6
0.5
0.4
0.3
0.2
0.1
0.0
Bias Voltage (V)
0.0
0.2
0.4
0.6
0.8
1.0
Pass-Thru State
Coupled State

FIG. 14

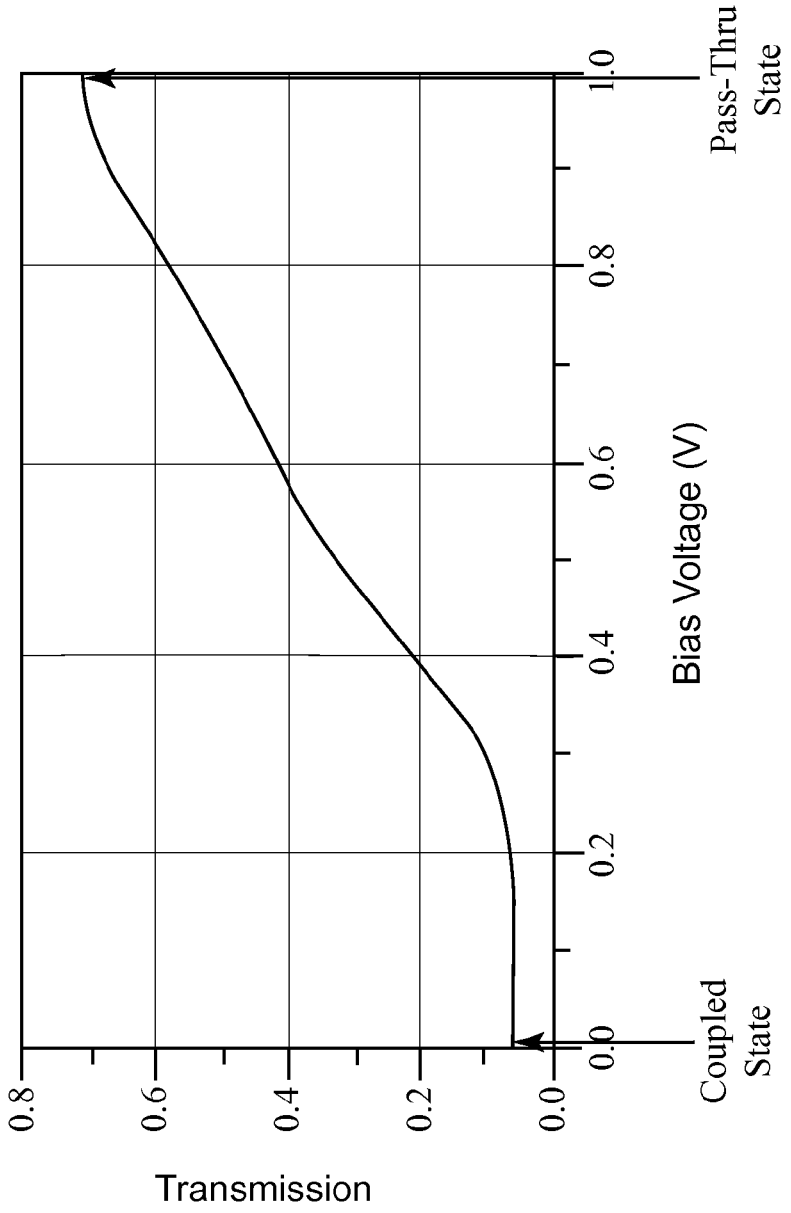
Transmission
0.0
0.2
0.4
0.6
0.8
Bias Voltage (V)
0.0
0.2
0.4
0.6
0.8
1.0
Coupled State
Pass-Thru State

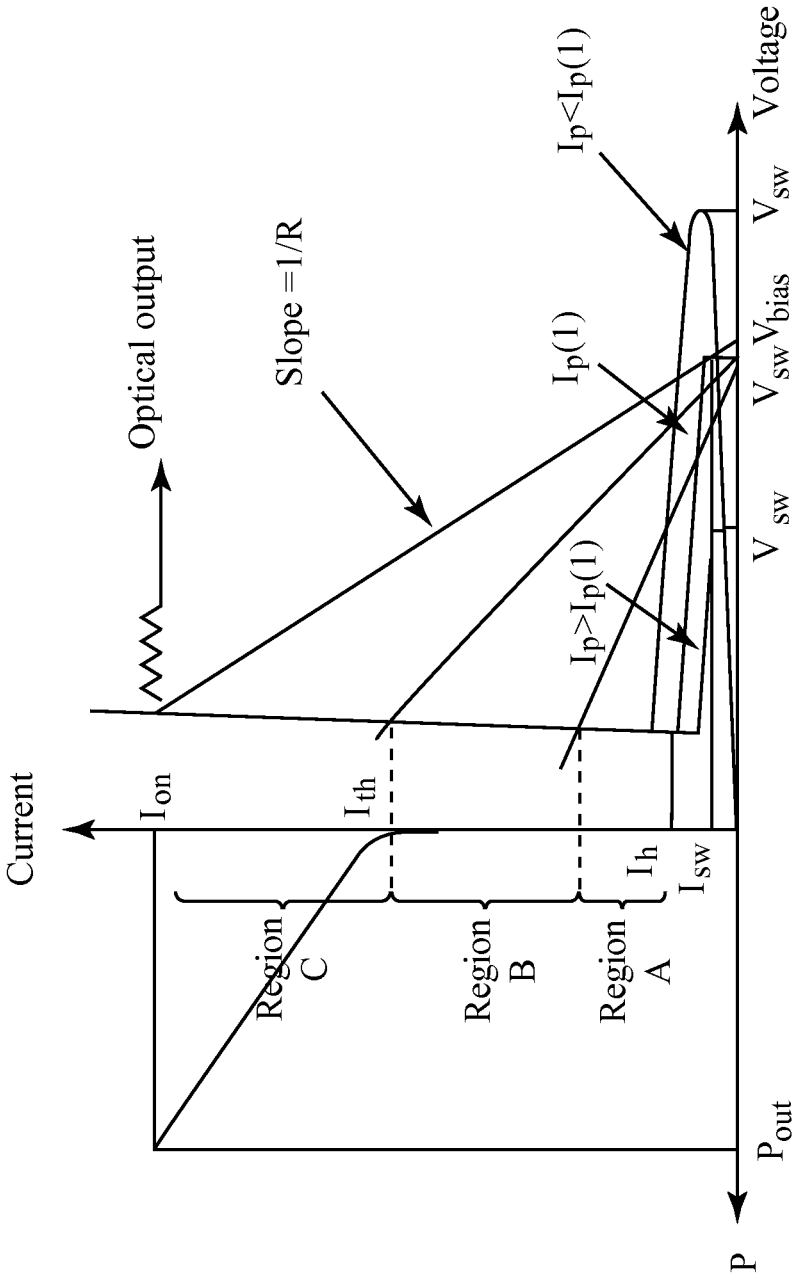
Current
Optical output
Slope =1/R
I_{on}
I_{th}
I_h
I_{sw}
$I_p(1)$
$I_p<I_p(1)$
$I_p>I_p(1)$
Region C
Region B
Region A
V_{sw}
V_{sw} V_{bias}
V_{sw}
Voltage
P
P_{out}

FIG. 15

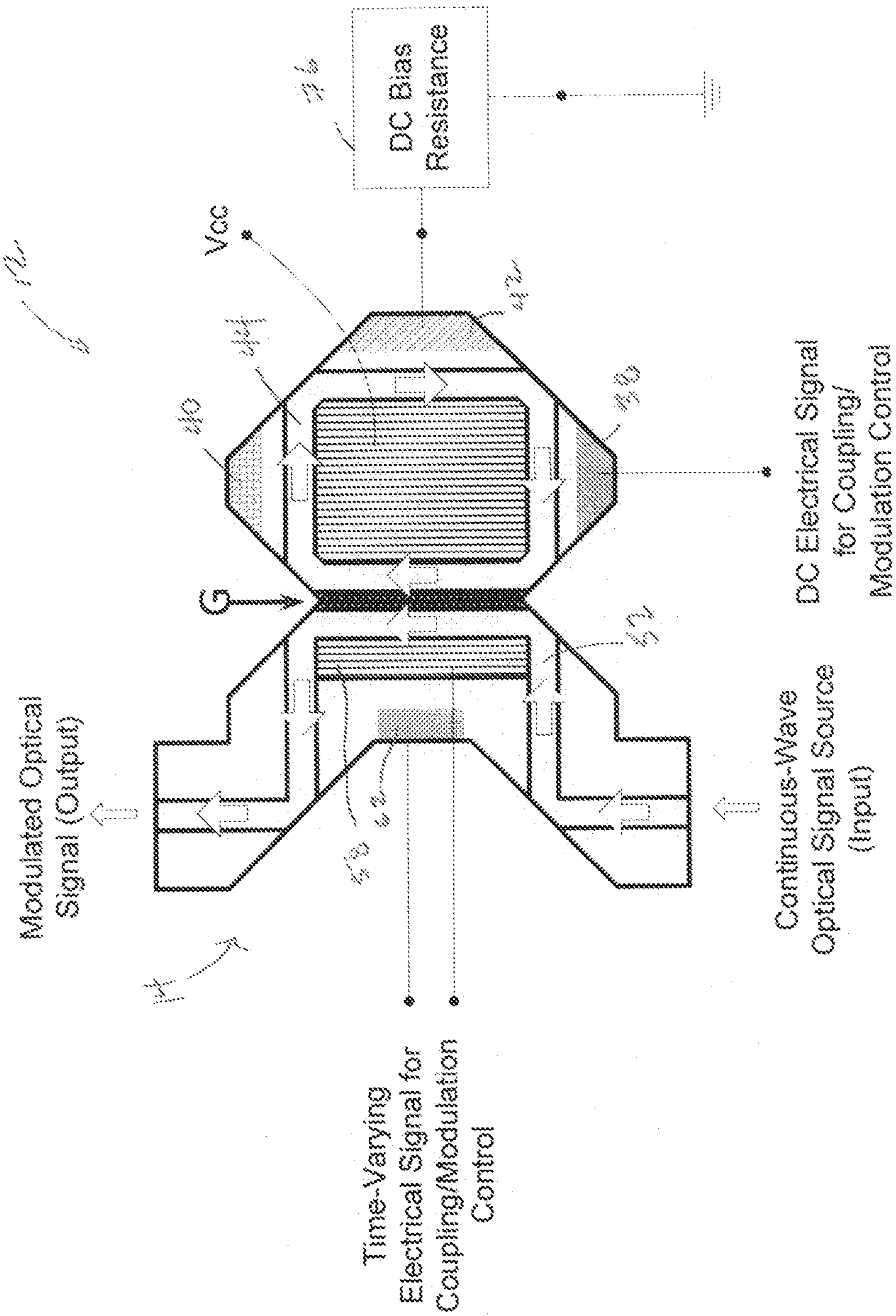
DC Bias Resistance
Vcc
G
DC Electrical Signal for Coupling/ Modulation Control
Modulated Optical Signal (Output)
Continuous-Wave Optical Signal Source (Input)
Time-Varying Electrical Signal for Coupling/Modulation Control

FIG. 16

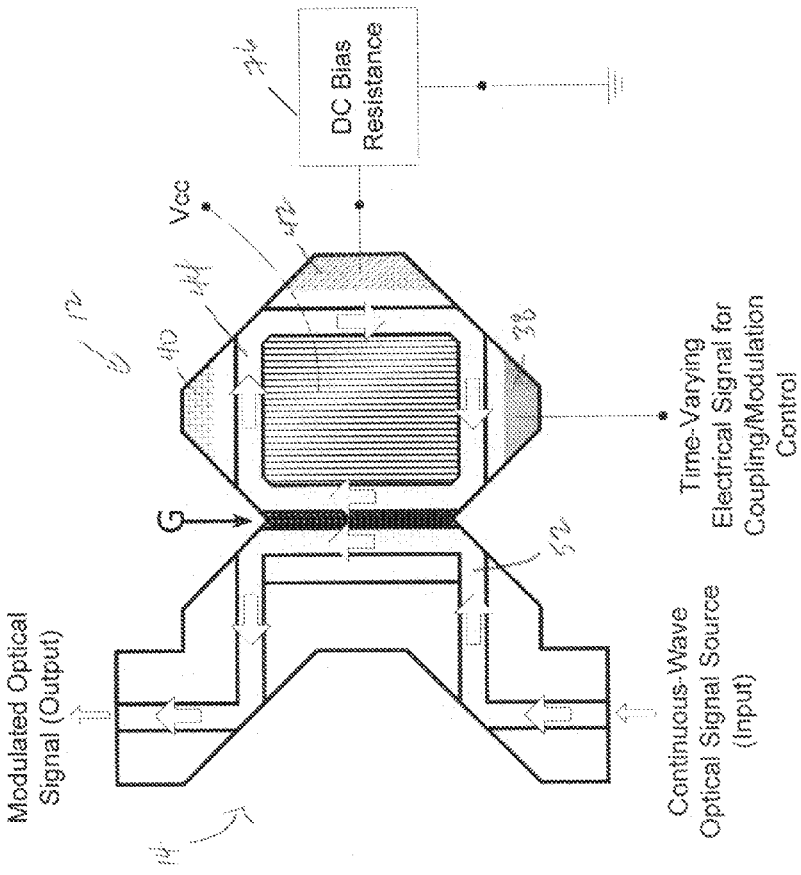
DC Bias Resistance
Vcc
G
Modulated Optical Signal (Output)
Continuous-Wave Optical Signal Source (Input)
Time-Varying Electrical Signal for Coupling/Modulation Control

FIG. 17

FIG. 18

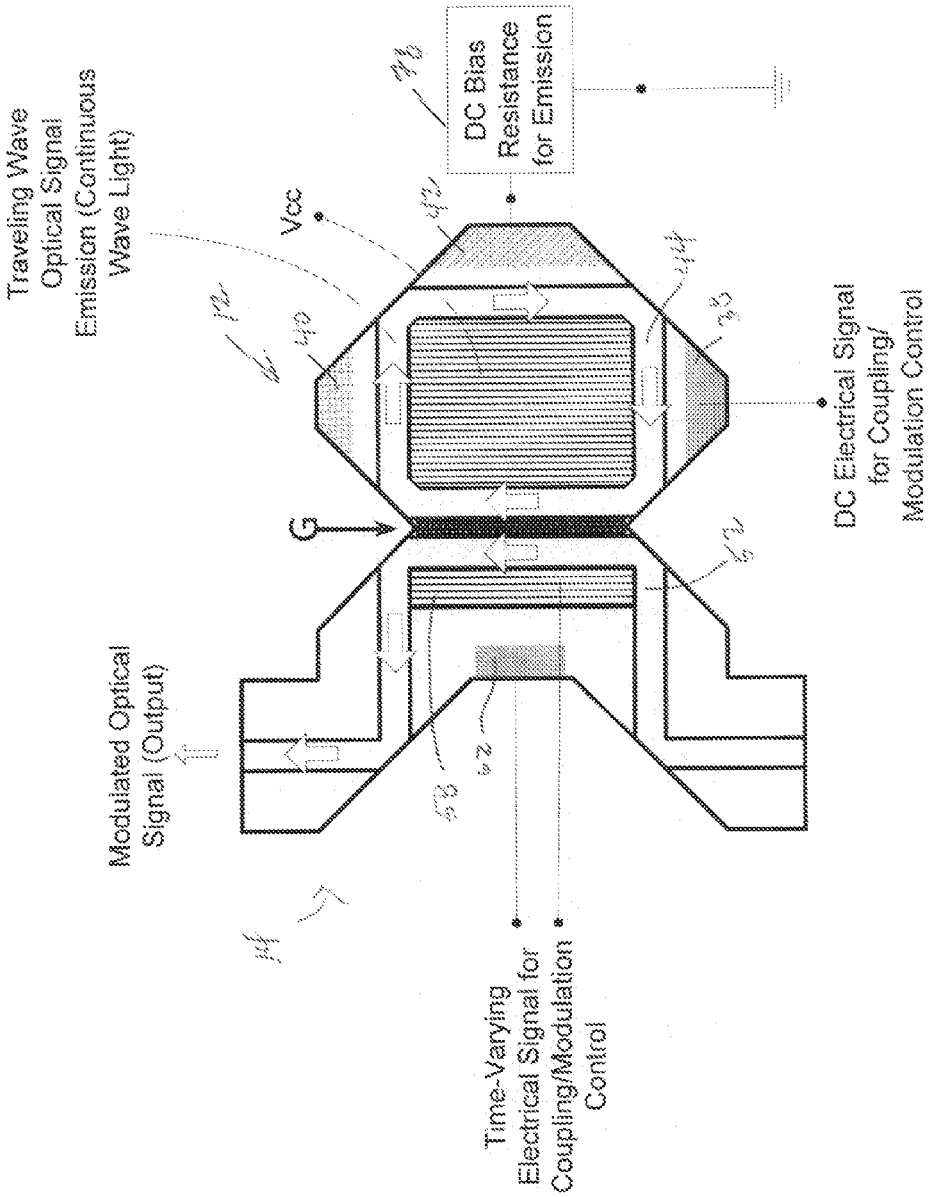
Traveling Wave Optical Signal Emission (Continuous Wave Light)
Vcc
DC Bias Resistance for Emission
DC Electrical Signal for Coupling/ Modulation Control
Modulated Optical Signal (Output)
Time-Varying Electrical Signal for Coupling/Modulation Control

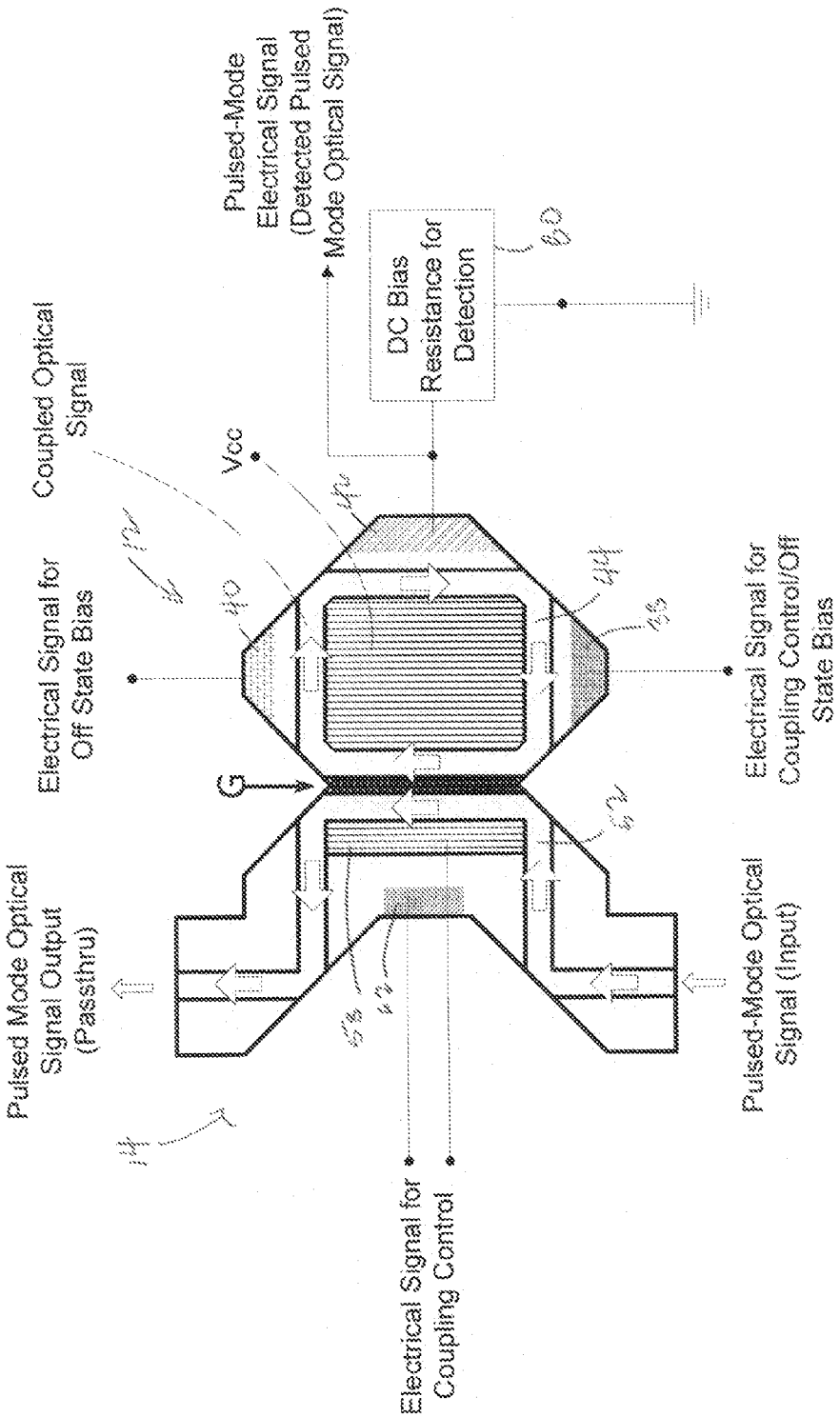
Pulsed-Mode Electrical Signal (Detected Pulsed Mode Optical Signal)
DC Bias Resistance for Detection
60
Coupled Optical Signal
Vcc
40
44
46
48
50
52
54
56
G
Electrical Signal for Off State Bias
Electrical Signal for Coupling Control/Off State Bias
Pulsed Mode Optical Signal Output (Passthru)
Pulsed-Mode Optical Signal (Input)
Electrical Signal for Coupling Control

FIG. 19

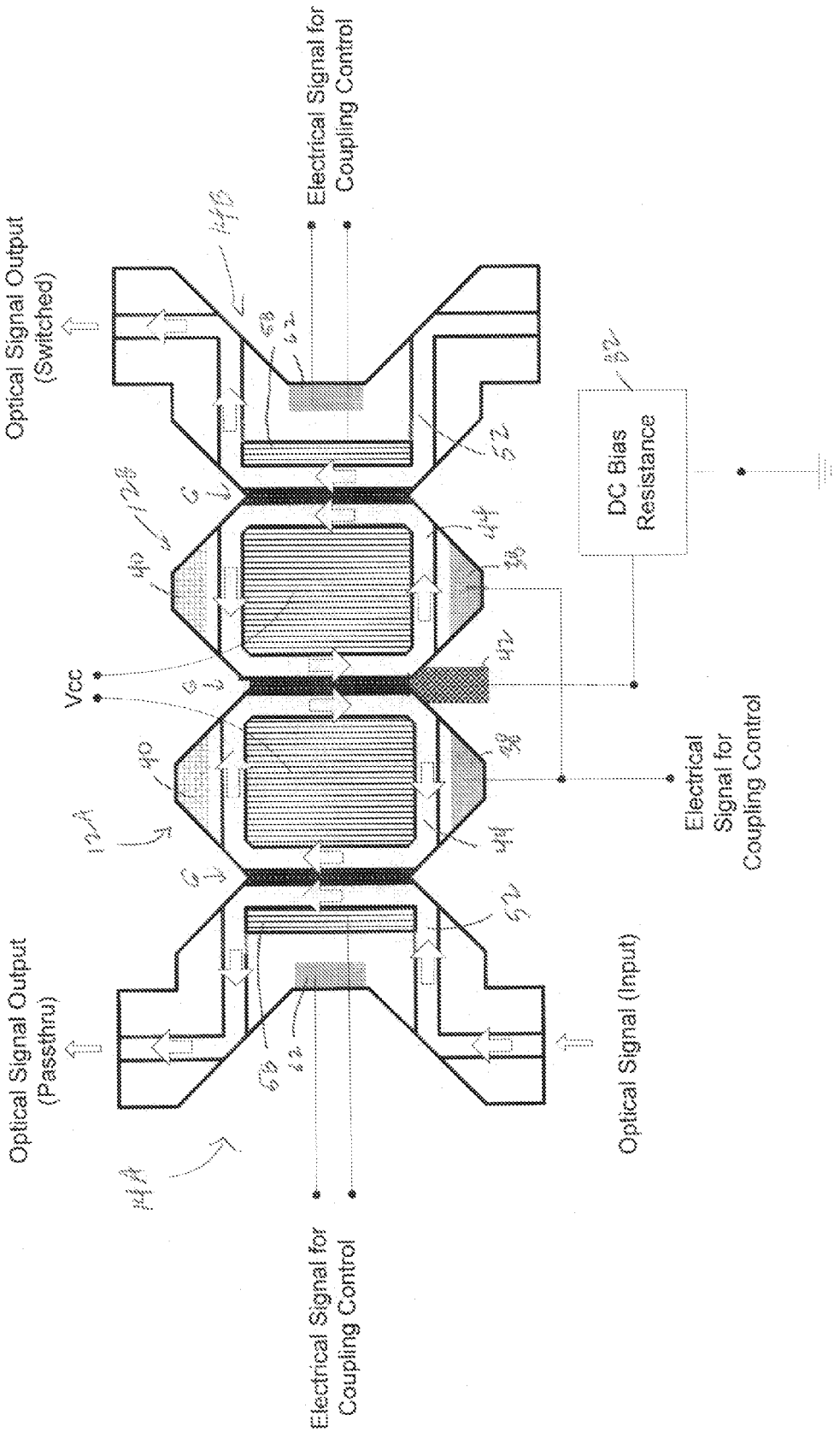
Optical Signal Output (Switched)
Electrical Signal for Coupling Control
DC Bias Resistance
Vcc
Electrical Signal for Coupling Control
Optical Signal Output (Passthru)
Optical Signal (Input)
Electrical Signal for Coupling Control

FIG. 20

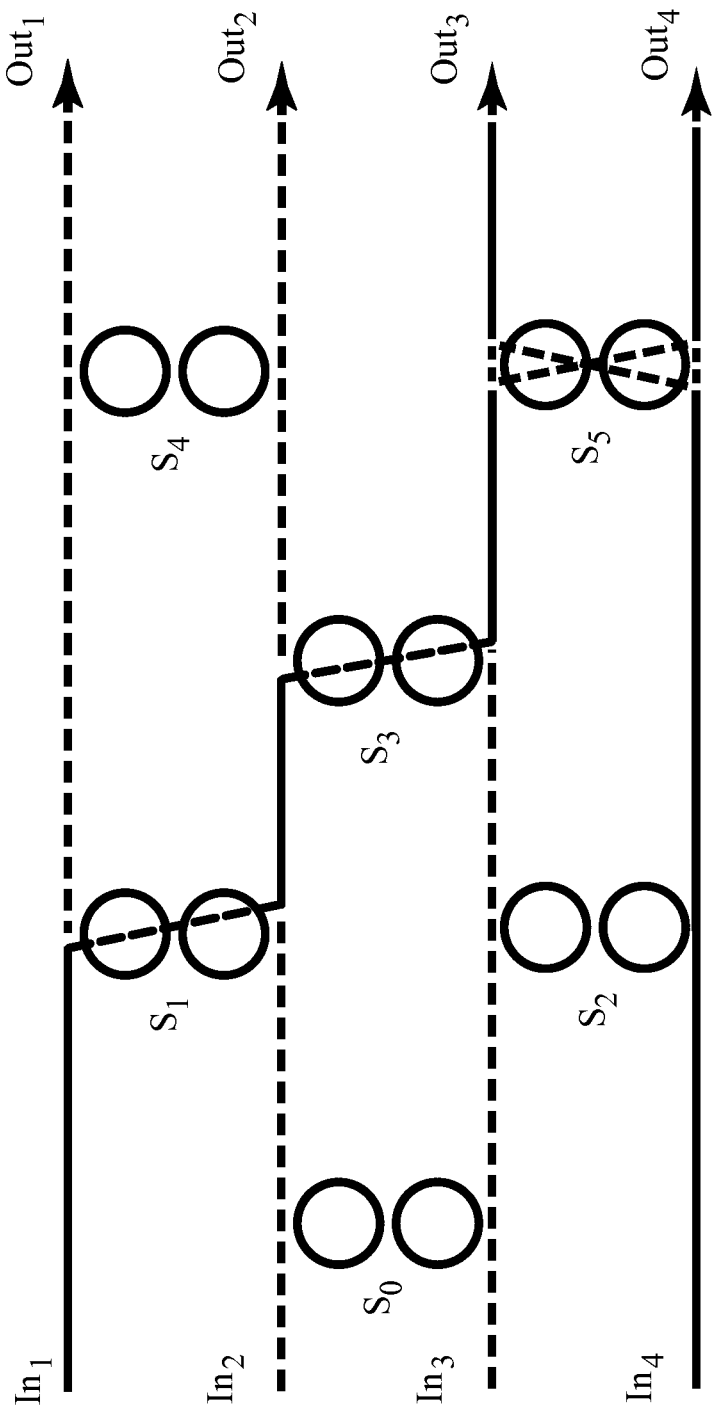

FIG. 21

FIG. 22

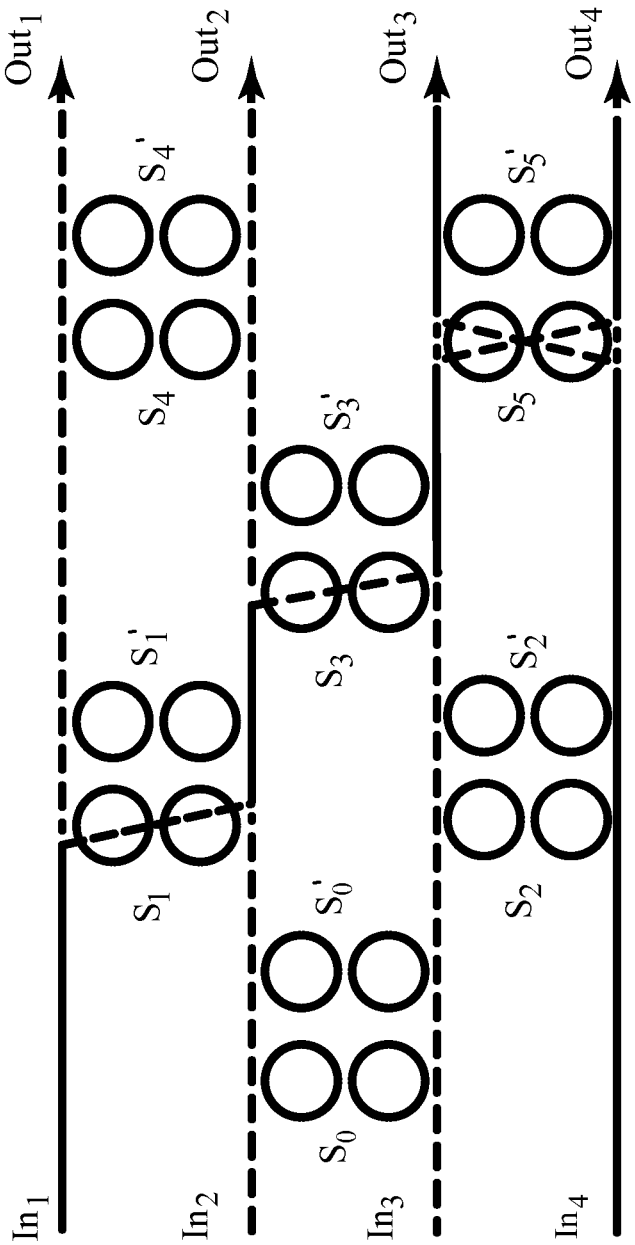
Out1
Out2
Out3
Out4
S4'
S4
S5'
S5
S3'
S3
S1'
S1
S2'
S2
S0'
S0
In1
In2
In3
In4

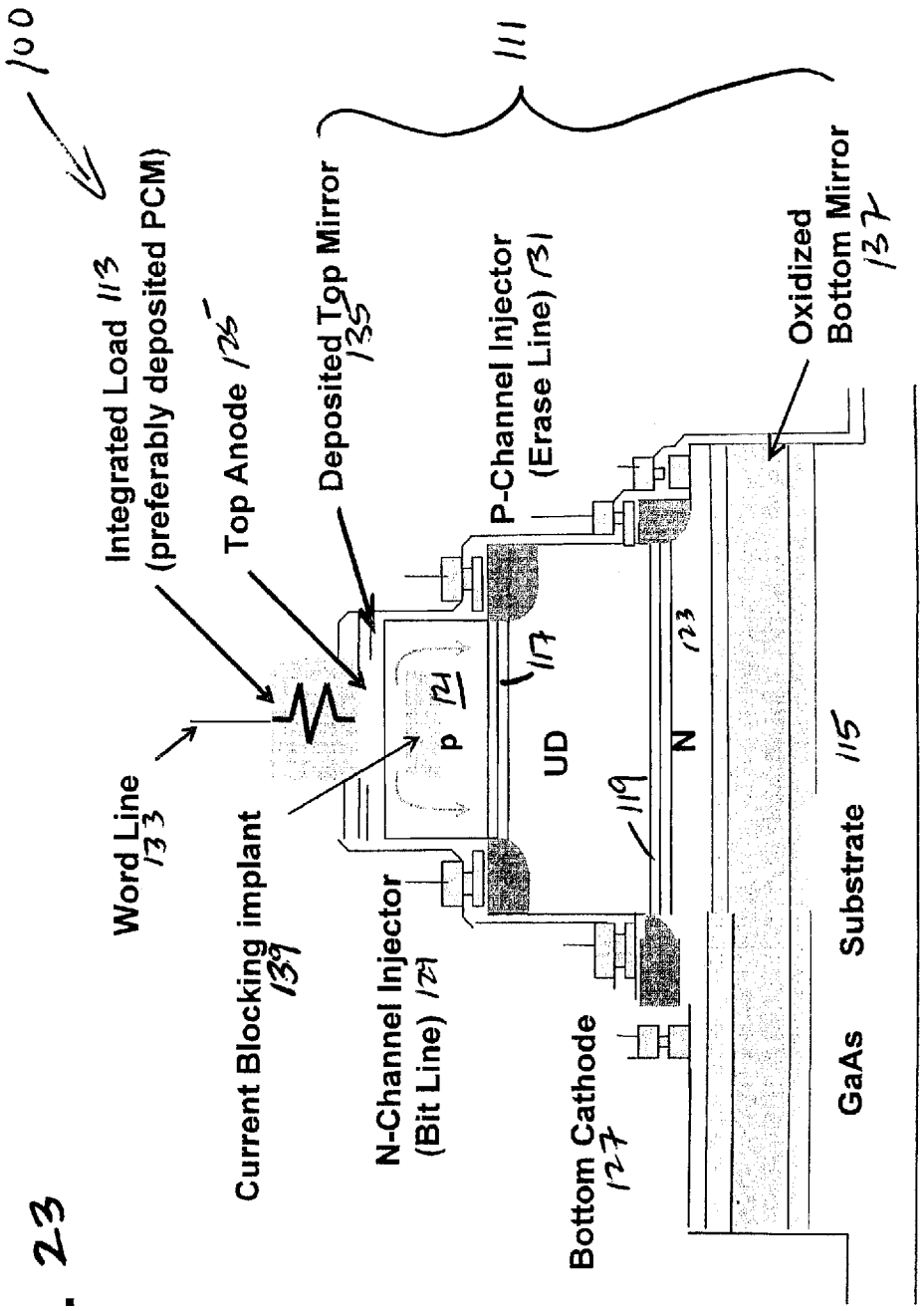
100
111
Integrated Load 113
(preferably deposited PCM)
Top Anode 125
Deposited Top Mirror 135
P-Channel Injector (Erase Line) 131
Oxidized Bottom Mirror 137
Word Line 133
Current Blocking implant 139
N-Channel Injector (Bit Line) 121
p 124
117
UD
119
N 123
Bottom Cathode 127
GaAs Substrate 115

FIG. 23

FIG. 24

Operations

- Write '1' : Electrical (or Optical)
- Write '0' : Electrical
- Read : Electrical (or Optical)
- NV Store ('1') : Electrical
- NV Erase ('0') : Electrical

FIG. 25

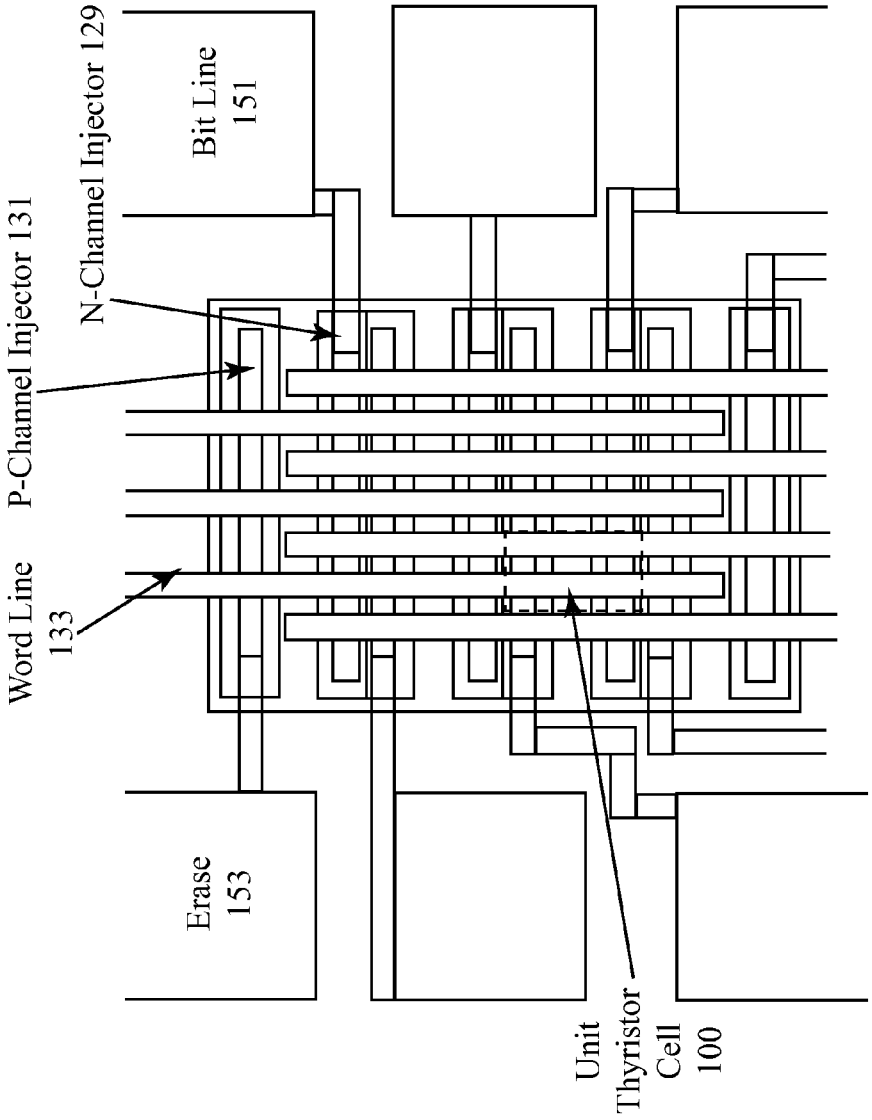
Bit Line
151
N-Channel Injector 129
P-Channel Injector 131
Word Line
133
Erase
153
Unit
Thyristor
Cell
100

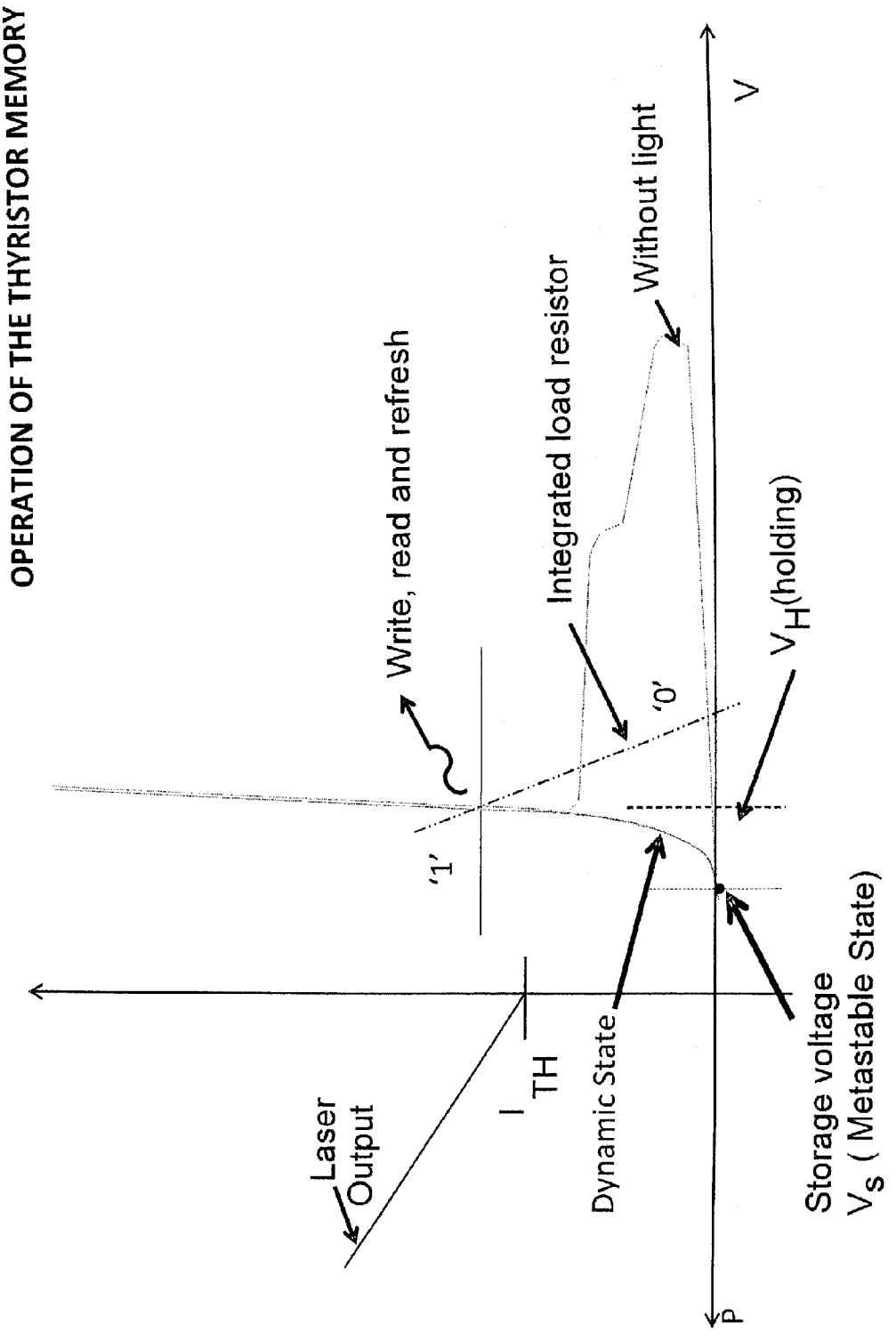
OPERATION OF THE THYRISTOR MEMORY
Write, read and refresh
Integrated load resistor
Without light
V
'1'
'0'
V_H(holding)
Laser Output
I_{TH}
Dynamic State
Storage voltage
V_S (Metastable State)
P

FIG. 26

FIG. 27 Static RAM Operation

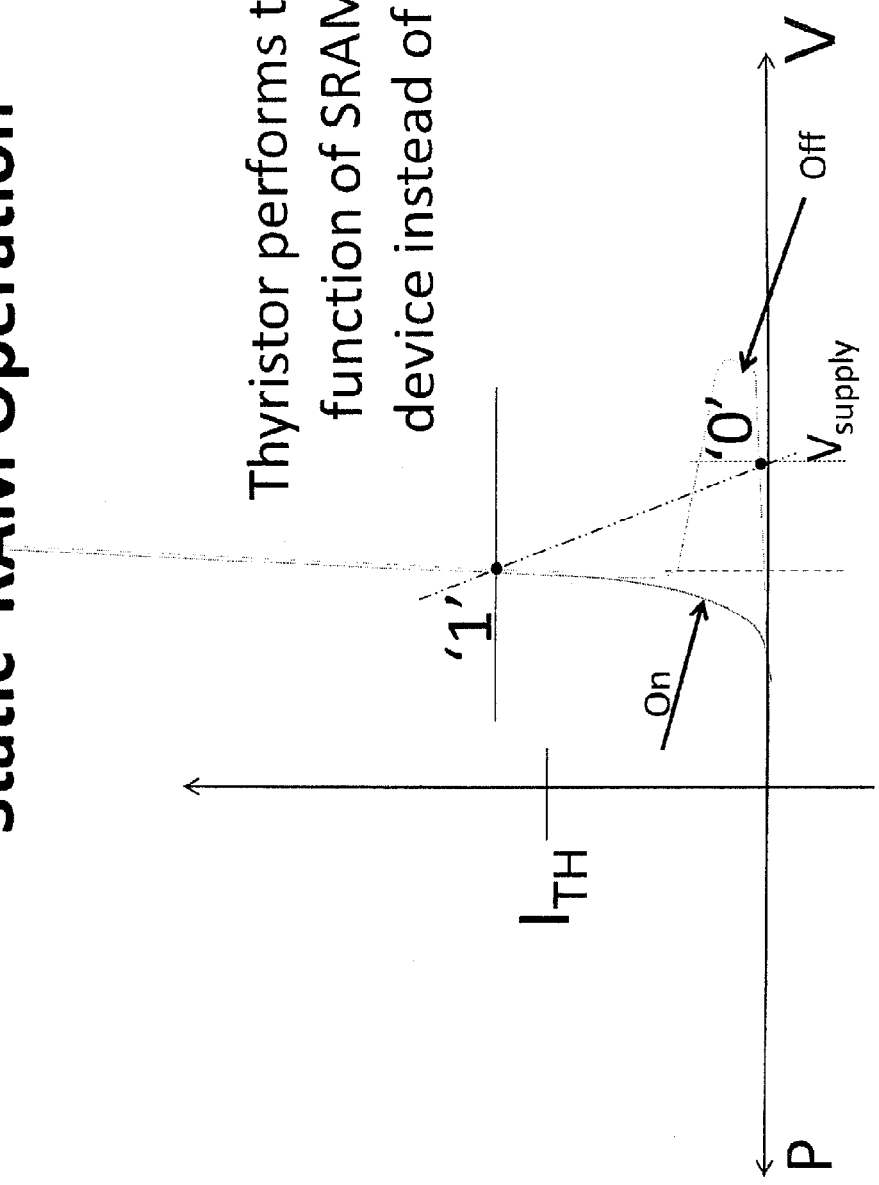

FIG. 28

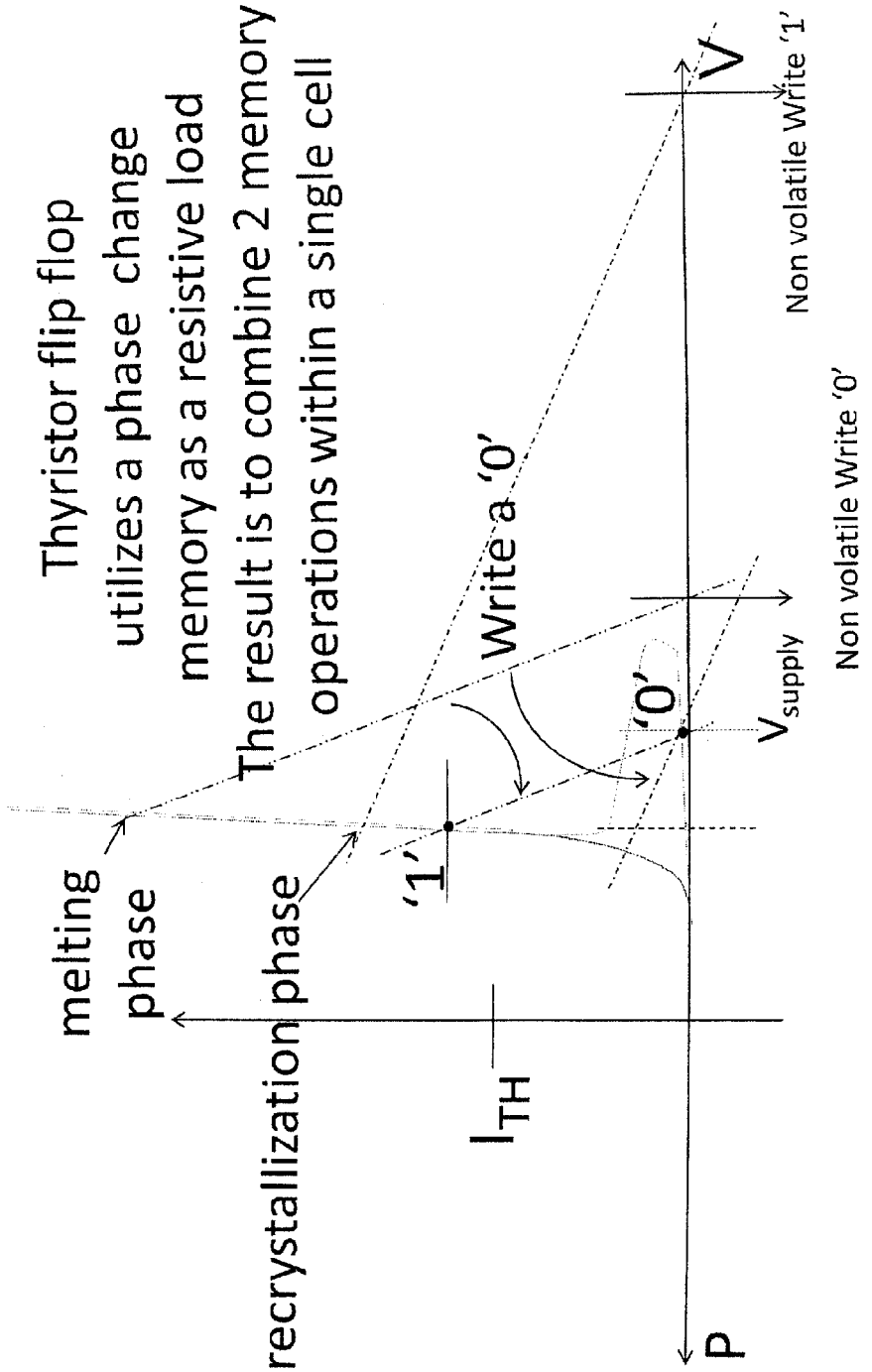
NV RAM Operation
Thyristor flip flop
utilizes a phase change
memory as a resistive load
The result is to combine 2 memory
operations within a single cell
melting
phase
recrystallization phase
'1'
Write a '0'
'0'
I_{TH}
V_{supply}
V
P
Non volatile Write '1'
Non volatile Write '0'

FIG. 29 **Dynamic RAM Operation**

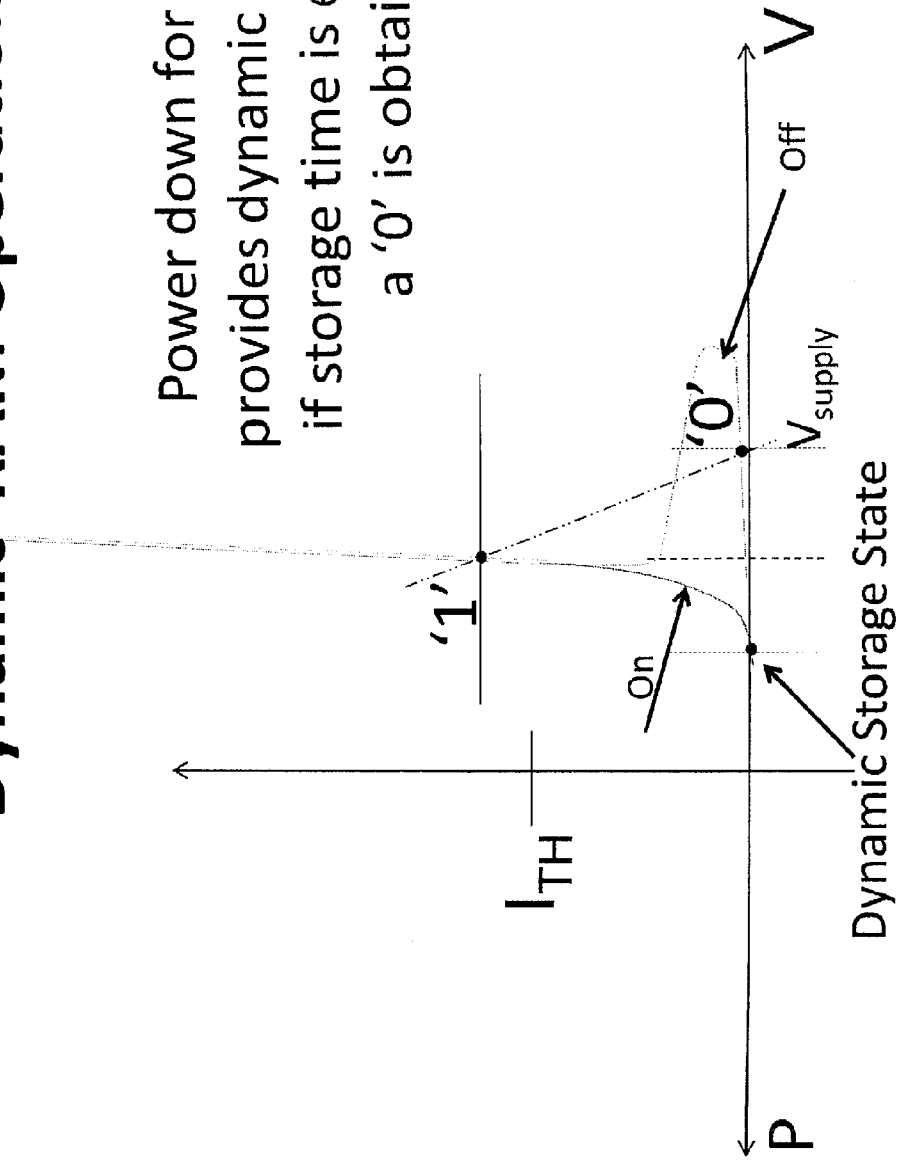

FIG. 30 STORAGE FUNCTION IN THE THYRISTOR MEMORY OPERATION

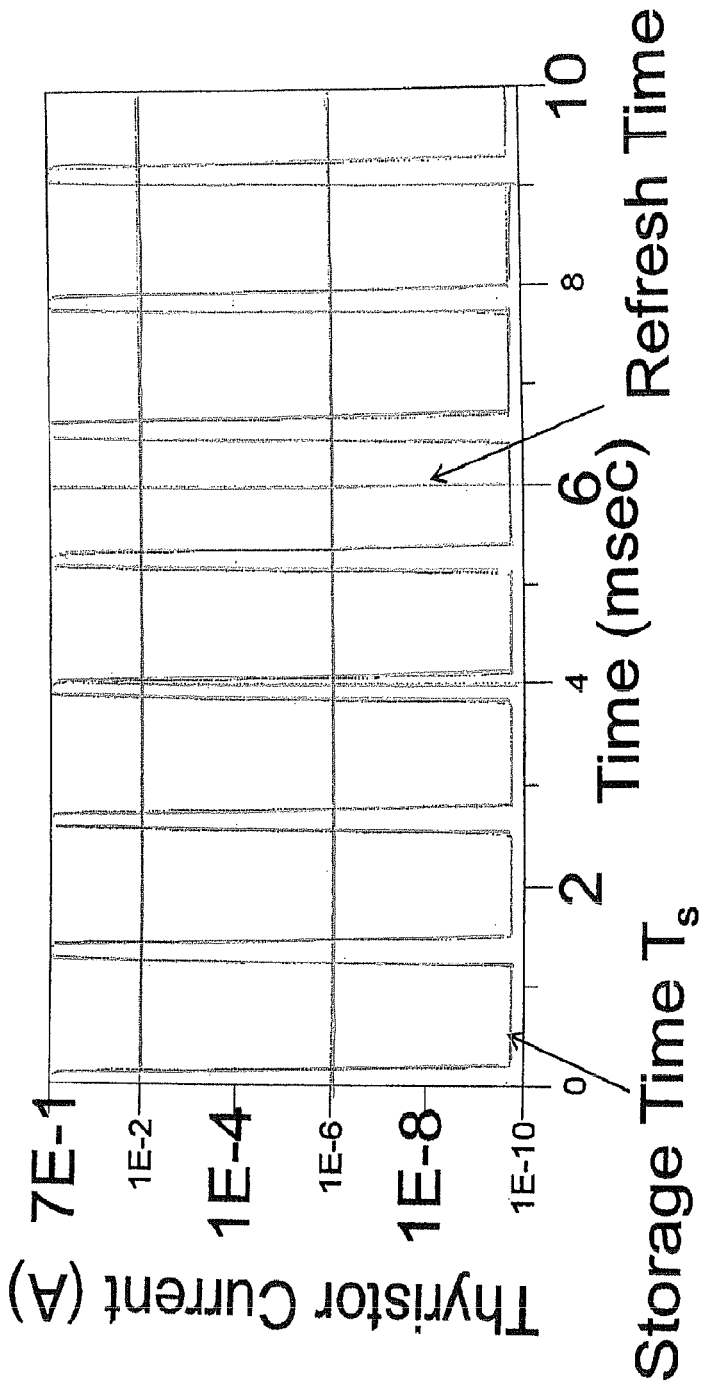

FIG. 31

Thyristor Memory Cell: Universal Memory Element

- A minimum size cell (crosspoint of an array) performs all memory functions → SRAM , DRAM or NV
- Mode of operation may be alternated between DRAM and SRAM to trade off speed for power
- NV operation can be enabled at any time, e.g. a decreasing power supply voltage could activate the NV write operation so that all data is captured
- Optoelectronic operation is utilized for specific applications such as photonic buffer memories
- Scaling superiority: thyristor/HFETs scale to <20nm nodes much more easily than CMOS because oxide scaling is eliminated
- Full compatibility with full spectrum of optical and optoelectronic circuit functions
- Advantage over Memristor a) only 1 polarity of voltage required
  b) optoelectronic compatible

OPTICAL CLOSED LOOP MICRORESONATOR AND THYRISTOR MEMORY DEVICE

BACKGROUND OF THE INVENTION

Optical ring resonator structures have been developed for optical modulation functions. Most of the proposed (and all of the demonstrated) optical ring resonator modulators are based on silicon-on-insulator (SOI) waveguides using silicon oxide cladding layers. The modulation relies on refractive index changes produced by the absorption of light in the intrinsic region of a p-i-n structure. Since the energy of the light at 1550 nm is less than the energy gap of the Si, then bandgap absorption is not allowed and the absorption must be enabled by the injection of both holes and electrons into the intrinsic region to create free carrier absorption.

One obvious drawback of these configurations is power consumption since relatively high voltages and current are required (the absorption is proportional to the current). Other drawbacks are the low values of absorption for a given current flow and the problem of removing the injected charge when the signal is reduced to zero.

SUMMARY

This summary is provided to introduce a selection of concepts that are further described below in the detailed description. This summary is not intended to identify key or essential features of the claimed subject matter, nor is it intended to be used as an aid in limiting the scope of the claimed subject matter.

The detailed description describes a monolithic semiconductor device that includes a waveguide structure optically coupled to an optical resonator. The optical resonator is adapted to process light at a predetermined wavelength. The optical resonator includes a closed loop waveguide having a plurality of straight sections that are optically coupled together by bend sections. The closed loop waveguide defines a central region surrounded by the closed loop waveguide. The waveguide structure includes a plurality of sections extending between an input and an output. One of the sections of the waveguide structure is spaced from and extends parallel to one straight section of the closed loop waveguide of the optical resonator to provide for evanescent-wave optical coupling therebetween. Both the optical resonator and the waveguide structure are formed in an epitaxial layer structure deposited on a substrate. The epitaxial layer structure includes at least one modulation doped quantum well interface. The central region of the optical resonator includes at least one ion implant that extends through the at least one modulation doped quantum well interface of the epitaxial layer structure. The at least one ion implant provides for lateral confinement of light within the closed loop waveguide. The at least one ion implant can also provide for funneling of DC current away from the central region and through the closed loop waveguide of the optical resonator.

The monolithic semiconductor device can be configured for a variety of functions, such as an optical modulator, in-plane laser, optical detector, and cross-point switching device as part of an optical switching fabric.

In one embodiment, the epitaxial layer structure includes complementary (both an n-type and a p-type) modulation doped quantum well interfaces formed between an n-type region and a p-type region to realize a thyristor structure.

In another embodiment, the closed loop waveguide is rectangular in nature with four straight sections coupled by ninety degree bends. Each ninety degree bend can include an outside facet and a cut inside corner that extends parallel to the outside facet, wherein the outside facet is defined a sidewall in the epitaxial layer structure and the cut inside corner is defined by the profile of the at least one ion implant. The waveguide structure can include a zig-zag structure with five straight sections coupled by ninety degree bends.

BRIEF DESCRIPTION OF THE DRAWINGS

FIG. **1** is a schematic perspective view of a monolithic optoelectronic device in accordance with the present invention; the monolithic optoelectronic device includes a zig-zag waveguide structure that is optically coupled by evanescent-wave coupling to a rectangular closed loop waveguide of a thyristor microresonator.

FIG. **2** is a schematic top view of the monolithic optoelectronic device of FIG. **1**.

FIGS. **3** and **4** are schematic cross-sectional views through sections A-A and B-B, respectively, of FIG. **2**, illustrating the exemplary device structure for realizing the thyristor microresonator and the zig-zag waveguide structure of the monolithic optoelectronic device of FIG. **1**.

FIG. **5**(A) is a schematic top view of a 90 degree bend of the rectangular closed path waveguide of the thyristor microresonator of FIG. **1**.

FIG. **5**(B) is an exemplary graph illustrating the variation in bend efficiency as a function of offset of the 90 degree bend of FIG. **5**(A).

FIG. **6** is an exemplary graph illustrating the variation in bend efficiency as a function of the gap width for the 90 degree bends of the coupling section of the zig-zag waveguide structure of FIG. **1**.

FIG. **7** is a schematic illustration of a mathematic model representing evanescent-wave coupling between the zig-zag waveguide structure and the rectangular closed path waveguide of the thyristor microresonator of FIG. **1**.

FIG. **8** is an exemplary graph illustrating the absorption coefficient α as a function of photon energy for the thyristor microresonator of FIG. **1** for two different differential bias voltages applied between the anode electrode and the n-channel injector electrode of the thyristor microresonator.

FIG. **9** is an exemplary graph illustrating the change of the absorption coefficient as a function of photon energy for the thyristor microresonator of FIG. **1** for the two different bias voltages shown in FIG. **8**.

FIG. **10** is an exemplary graph illustrating the change in refractive index as a function of photon energy for the thyristor microresonator of FIG. **1** for the two different bias voltages shown in FIG. **8**.

FIG. **11** is a graph of the absorption coefficient α as a function of differential bias voltage applied between the anode electrode and the n-channel injector electrode for an exemplary thyristor microresonator structure.

FIG. **12** is a graph illustrating the change in refractive index as a function of differential bias voltage applied between the anode electrode and the n-channel injector electrode for the exemplary thyristor microresonator of FIG. **11**.

FIG. **13** is a graph illustrating optical signal transmission through the zig-zag waveguide as a function of differential bias voltage applied between the anode electrode and the n-channel injector electrode of the exemplary thyristor microresonator of FIG. **11**.

FIG. **14** is a graph illustrating optical signal transmission through the zig-zag waveguide as a function of differential bias voltage applied between the top electrode and the

n-channel electrode of the zig-zag waveguide structure for an exemplary thyristor microresonator and zig-zag waveguide structure.

FIG. **15** is an exemplary I-V-P curve illustrating a number of operational modes as a function of bias resistance for the thyristor microresonator of the present invention.

FIG. **16** is a schematic top view of an exemplary configuration of the monolithic optoelectronic device of FIG. **1** as an optical modulator.

FIG. **17** is a schematic top view of another exemplary configuration of the monolithic optoelectronic device of FIG. **1** as an optical modulator.

FIG. **18** is a schematic top view of an exemplary configuration of the monolithic optoelectronic device of FIG. **1** as an in-plane laser.

FIG. **19** is a schematic top view of an exemplary configuration of the monolithic optoelectronic device of FIG. **1** as an optical detector.

FIG. **20** is a schematic top view of a monolithic optical switch device utilizing two pairs of a thyristor microresonator and optically-coupled zig-zag waveguide structure; the thyristor microresonators are also optically coupled to one another by evanescent-wave coupling.

FIG. **21** is a schematic view of a switch fabric utilizing a number of the optical switch devices of FIG. **20**.

FIG. **22** is a schematic view of another switch fabric utilizing a number of the optical switch devices of FIG. **20**; the switch fabric of FIG. **22** is suitable for wavelength division multiplexing applications where optical input signals of different wavelengths are switched between the input and output ports of the switch fabric.

FIG. **23** is a schematic diagram of a thyristor memory cell according to the present invention.

FIG. **24** is a diagram summarizing the operations of the thyristor memory cell of FIG. **23**.

FIG. **25** is a schematic view of an array of thyristor memory cells of FIG. **23** integrated on a common substrate.

FIG. **26** is an exemplary IV curve illustrating the operations of the thyristor memory cell of FIG. **23**.

FIG. **27** is an exemplary IV curve illustrating the static RAM operations of the thyristor memory cell of FIG. **23**.

FIG. **28** is an exemplary IV curve illustrating the non-volatile RAM operations of the thyristor memory cell of FIG. **23**.

FIG. **29** is an exemplary IV curve illustrating the dynamic RAM operations of the thyristor memory cell of FIG. **23**.

FIG. **30** is an exemplary diagram of storage function of the thyristor memory cell of FIG. **23** for dynamic RAM operations.

FIG. **31** is a diagram summarizing the benefits of the thyristor memory cell of FIG. **23**.

DETAILED DESCRIPTION OF ILLUSTRATIVE EMBODIMENTS

The present application builds upon Planar Optoelectronic Technology (POET) that provides for the realization of a variety of devices (optoelectronic devices, logic circuits and/or signal processing circuits) utilizing inversion quantum-well channel device structures as described in detail in U.S. Pat. No. 6,031,243; U.S. patent application Ser. No. 09/556,285, filed on Apr. 24, 2000; U.S. patent application Ser. No. 09/798,316, filed on Mar. 2, 2001; International Application No. PCT/US02/06802 filed on Mar. 4, 2002; U.S. patent application Ser. No. 08/949,504, filed on Oct. 14, 1997, U.S. patent application Ser. No. 10/200,967, filed on Jul. 23, 2002; U.S. application Ser. No. 09/710,217, filed on Nov. 10, 2000; U.S. Patent Application No. 60/376,238, filed on Apr. 26, 2002; U.S. patent application Ser. No. 10/323,390, filed on Dec. 19, 2002; U.S. patent application Ser. No. 10/280,892, filed on Oct. 25, 2002; U.S. patent application Ser. No. 10/323,390, filed on Dec. 19, 2002; U.S. patent application Ser. No. 10/323,513, filed on Dec. 19, 2002; U.S. patent application Ser. No. 10/323,389, filed on Dec. 19, 2002; U.S. patent application Ser. No. 10/323,388, filed on Dec. 19, 2002; U.S. patent application Ser. No. 10/340,942, filed on Jan. 13, 2003; all of which are hereby incorporated by reference in their entireties. These device structures are built from an epitaxial layer structure and associated fabrication sequence that can be used to make the devices on a common substrate. In other words, n type and p type contacts, critical etches, etc. can be used to realize one or more of the devices simultaneously on a common substrate. Features of the epitaxial structure include 1) a bottom n-type layer structure, 2) a top p-type layer structure, and 3) an n-type modulation doped quantum well interface and a p-type modulation doped quantum well interface disposed between the bottom n-type layer structure and the top p-type layer structure. N-type and p-type ion implants are used to contact the n-type and p-type modulation doped quantum well interfaces, respectively. N-type metal contacts to the n-type ion implants and the bottom n-type layer structure. P-type metal contacts to the p-type ion implants and the top p-type layer structure. The epitaxial layer structure can be realized with a material system of group III-V materials (such as a GaAs/AlGaAs). The n-type modulation doped quantum well interface includes a relatively thin layer of highly doped n-type material (referred to herein as an "n+ charge sheet") spaced from one or more quantum wells by an undoped spacer layer. The p-type modulation doped quantum well interface includes a relatively thin layer of highly doped p-type material (referred to herein as a "p+ charge sheet") spaced from one or more quantum wells by an undoped spacer layer. The n+ charge sheet is disposed above the quantum well(s) of the n-type modulation doped quantum well interface adjacent the top p-type layer structure. The p+ charge sheet is disposed below the quantum well(s) of the p-type modulation doped quantum well interface adjacent the bottom n-type layer structure. One or more spacer layers are disposed between the quantum well(s) of the n-type modulation doped quantum well interface and the one or more quantum well(s) of the p-type modulation doped quantum well interface. A bottom dielectric distributed Bragg reflector (DBR) mirror can be formed below the bottom n-type layer structure. The bottom DBR mirror can be formed from alternating layers of AlAs and GaAs. The AlAs layers are subjected to high temperature steam oxidation to produce the compound Al_xO_y so as to form the bottom DBR mirror. A top dielectric mirror can be formed above the top p-type layer structure. The top dielectric mirror can be formed from alternating layers of SiO_2 and a high refractive index material such as silicon or titanium dioxide (TiO_2). The bottom and top mirrors provide for vertical confinement of light. The top dielectric mirror can cover the sidewalls of the device structure to provide for lateral confinement of light as needed.

POET can be used to construct a variety of high performance transistor devices, such as complementary NHFET and PHFET unipolar devices as well as n-type and p-type HBT bipolar devices. POET can also be used to construct a variety of optoelectronic devices which include:

a thyristor VCSEL laser;
an NHFET laser;
an PHFET laser;
a thyristor optical detector;
an NHFET optical detector;

an PHFET optical detector;

a semiconductor optical amplifier (SOA) or a linear optical amplifier (LOA) based on either one (or both) of the n-type and p-type quantum well interfaces;

an absorption (intensity) optical modulators based on either one (or both) of the n-type and p-type quantum well interfaces;

a phase modulator based on either one (or both) of the n-type and p-type quantum well interfaces;

a waveguide switch; and

a passive waveguide.

The present invention extends the POET device structure to allow for the construction of a monolithic optoelectronic device including a thyristor microresonator **12** that is spaced from a section of a zig-zag waveguide structure **14** by a gap region G. The zig-zag waveguide structure **14** is optically coupled to the thyristor microresonator **12** by evanescent-wave coupling over the gap region G as will be described in detail below.

In an exemplary embodiment, the thyristor microresonator **12** is realized from an active device structure that includes a bottom DBR mirror **16** formed on a substrate **18** (such as a GaAs wafer) as best shown in the cross-sections of FIGS. **3** and **4**. A bottom n-type layer structure **20** (such as a layer **20***a* of n+ GaAs and a layer **20***b* of n+AlGaAs) is formed above the DBR mirror **16**. The bottom DBR mirror **16** can be formed from alternating layers of AlAs and GaAs. The AlAs layers are subjected to high temperature steam oxidation to produce the compound Al_xO_y so as to form the bottom DBR mirror **16**. A p-type modulation doped quantum well interface **22** is formed above the n-type layer structure. The p-type modulation doped quantum well interface **22** includes a p+ charge sheet spaced from one or more quantum wells by an undoped spacer layer. The p+ charge sheet is disposed below the quantum well(s) of the p-type modulation doped quantum well interface **22** adjacent the bottom n-type layer structure **20**. One or more undoped spacer layers (such as layers **24***a* and undoped AlGaAs layer **24***b*) are formed above the p-type modulation doped quantum well interface **22**. An n-type modulation doped quantum well interface **26** is formed above the undoped spacer layer(s) **24**. The n-type modulation doped quantum well interface **26** includes an n+ charge sheet spaced from one or more quantum wells by an undoped spacer layer. A top p-type layer structure **28** (such as layers **28***a*, **28***b* of P+ AlGaAs, and **28***c*) is formed above the n-type quantum well interface **26**. The n+ charge sheet is disposed above the quantum well(s) of the n-type modulation doped quantum well interface adjacent the top p-type layer structure **28**. A refractory p-type anode electrode **30** is formed on the top p-type layer structure **28**. A top dielectric mirror **32** is formed above the top p-type layer structure **28** and the refractory anode **30**. The top dielectric mirror **32** can be formed from alternating layers **32***a*, **32***b* of SiO_2 and a high refractive index material such as silicon. The top dielectric mirror **32** can cover the sidewalls of the device structure as shown to provide for lateral confinement of light as needed. An n-type ion implant **34** into a mesa above the n-type modulation doped quantum well interface **26** is used to contact the n-type modulation doped quantum well interface **26**. A p-type ion implant **36** into a mesa above the p-type modulation doped quantum well interface **22** is used to contact the p-type modulation doped quantum well interface **22**. N-type metal **38** contacts to the n-type ion implant **34** to form an n-channel injector electrode that is electrically coupled to the n-type modulation doped quantum well interface **26**. P-type metal **40** contacts to the p-type ion implants **36** to form an n-channel injector electrode that is electrically coupled to the p-type modulation doped quantum well interface **22**. N-type metal **42** is deposited on a mesa formed in the bottom n-type layer structure **20** (such as the bottom layer **20***a*) to form a cathode electrode of the device.

Details of exemplary epitaxial layers and fabrication methodology to realize the device structure of the thyristor microresonator **12** are described in POET patents as incorporated by reference above.

As best shown in FIGS. **1** and **2**, the thyristor microresonator **12** defines a waveguide **44** that follows a closed path that is generally rectangular in shape. The optical mode circulates around the waveguide **44** and is strongly confined within the waveguide **44** by internal reflection at the reflective interfaces of the waveguide **44**. More specifically, vertical confinement of the optical mode in the waveguide **44** is provided by the bottom DBR mirror **16** and the top dielectric mirror **32** (layers **32***a*, **32***b*) as shown in the cross-sections of FIGS. **3** and **4**. Lateral confinement of the optical mode in the waveguide **44** is provided by a refractive index change at the sidewalls **46** that define the outer boundary of the waveguide **44** (FIGS. **1**, **2**, **3** and **4**) and by refractive index change at the periphery of the implant regions **48***a*, **48***b* under the top anode electrode **30** (FIGS. **3** and **4**). Lateral confinement of the optical mode in the waveguide **44** can also be aided by the top dielectric mirror **32** that covers the sidewalls **46** as shown. The central implant regions **48***a*, **48***b* are of suitable n+ material and can be formed by localized implantation of a suitable n+ species (such as silicon fluoride ions) into the device structure prior to deposition and patterning of the top refractory p-type anode electrode **30**. The perimeters of the central implant regions **48***a*, **48***b* are generally rectangular in shape and define the inner reflective surface of the waveguide **44**. The depths of the central implant regions **48***a*, **48***b* (which is controlled by the power level during implantation) encompass the n-type and p-type modulation doped quantum well interfaces **22** and **26**, respectively. The central implant regions **48***a* and **48***b* act as a barrier to current flow so as to funnel current flowing between the anode electrode **30** and the cathode electrode **40** into the active region (show as dotted line **49**) of the waveguide **44** and away from the central region of the device below the top anode electrode **30**. The operation of the thyristor microresonator **12** relies on electrical signals supplied to the electrodes of the device (e.g., the top anode electrode **30**, the n-channel injector electrode **38**, the p-channel injector electrode **40**, and the bottom cathode electrode **42**) as is described below in detail.

The length of the closed path waveguide **44** is tuned to the particular wavelength of the optical mode that is to propagate in the waveguide **44**. More specifically, the length of the rectangular closed path waveguide **44** is given as $2(L_1+L_2)$ for the L_1 and L_2 length parameters of the waveguide **44** as best shown in FIG. **2**. In this configuration, the L_1 and L_2 parameters are selected to conform to the following:

$$2(L_1 + L_2) = \frac{2\pi m\lambda}{n_{eff}} \quad (1)$$

where L_1 and L_2 are the effective lengths of the opposed sides of the closed path waveguide **44**;

m is an integer greater than zero;

λ is the wavelength of the optical mode that is to propagate in the waveguide **44**; and

n_{eff} is the effective refractive index of the waveguide **44**.

The width (W) of the closed path waveguide **44** can be less than 2 μm, and possibly 1 μm or less. The width of the gap

region G (i.e., the spacing between the waveguide **44** and the waveguide structure **14**) can be less than 2 μm, and possibly on the order of 1 μm.

The rectangular closed path waveguide **44** of the thyristor microresonator **12** is formed by four ninety degree bends. As best shown in FIGS. **1**, **2** and **5**(A), each ninety degree bend is defined by a respective forty-five degree facet **50** formed in the outer sidewall **46** of the waveguide **44**. The rectangular waveguide **44** has several advantages, including but not limited to: 1) it allows for the four separate contacts to the electrodes of the thyristor device structure; 2) it allows the width of the waveguide **44** to be greater than the resonant wavelength, and thus reduces the dimensional tolerances and associated manufacturing complexities required for smaller resonance wavelengths (such as wavelengths at or near 1 μm); 3) it allows for effective control over the width of the waveguide **44** as well as the gap width between the waveguide **44** and the waveguide structure **14**—these two parameters influence the Q factor of the thyristor microresonator **12** and the efficiency of the evanescent-wave coupling between the two waveguides; and 4) it provides a high packing density in laying out the structures on the substrate.

In one embodiment as best shown in FIG. **5**(A), the inside corner of each respective ninety degree bend of the rectangular waveguide **44** is cut (or blunted) by a facet **51** that is oriented substantially parallel to the four-five degree facet **50** of the respective bend. The cut inside corner of each respective ninety degree bend improves the bend efficiency, which provides for improved resonance of the optical mode traveling wave propagating around the rectangular waveguide **44**. The length and position of the cut inside corner (facet **51**) relative to the four-five degree facet **50** of the respective bend can be characterized by an offset parameter as shown in FIG. **5**(A). The offset parameter of the cut inside corner (and thus the length and position of the cut inside corner (facet **51**) relative to the four-five degree facet **50**) can be varied by design and can affect the bend efficiency of the ninety degree bends as a function of width of the waveguide **44** as shown in FIG. **5**(B). Bend efficiency is the ratio of the optical power in the waveguide after bend relative to optical power incident on the bend. In this illustrative embodiment, an offset parameter of 0.2 μm is best used for a rectangular waveguide **44** of a width of 2 μm or less, while other offset parameters can be used for other widths. The cut inside corners (facet **51**) are defined by the profile of the central implant regions **48***a*, **48***b*, which is dictated by the mask used for the ion implantation that forms the central implant regions **48***a*, **48***b*.

As best shown in FIGS. **1**, **2** and **4**, the waveguide structure **14** defines a rib waveguide **52** that forms a zig-zag path. The optical mode is strongly confined within the waveguide **52** by internal reflection at the reflective interfaces of the waveguide **52**. More specifically, vertical confinement of the optical mode in the waveguide **52** is provided by the bottom DBR mirror **16** and the top dielectric mirror **32** (layers **32***a*, **32***b*) as shown in the cross-sections of FIGS. **3** and **4**. Lateral confinement of the optical mode in the waveguide **52** is provided by refractive index changes at the opposed sidewalls **54***a*, **54***b* of the waveguide **52** (FIGS. **1**, **2**, and **4**).

In the coupling region (FIG. **7**), the waveguide **52** includes a section that extends parallel to and is closely-spaced from a straight section of the microresonator waveguide **44** by the gap region G. In this section of the waveguide **52**, lateral confinement of the optical mode is provided by a refractive index change provided by at the periphery of the implant regions **56***a*, **56***b* under a top p-type refractory electrode **58** (FIG. **4**). The implant regions **56***a*, **56***b* are of suitable n+ material and can be formed by localized implantation of a suitable n+ species (such as silicon fluoride ions) into the device structure prior to deposition and patterning of the top refractory electrode **58**. The depths of the implant regions **56***a*, **56***b* (which is controlled by the implant energy during implantation) encompass the n-type and p-type modulation doped quantum well interfaces **22** and **26**, respectively. The implant regions **56***a*, **56***b* can be formed along with the implant regions **48***a*, **48***b* of the thyristor microresonator **12**. The top refractory electrode **58** can be deposited and patterned along with the top p-type anode electrode **30** of the thyristor microresonator **12**. Lateral confinement of the optical mode in the waveguide **52** an also be aided by the top dielectric mirror **32** (layers **32***a*, **32***b*) formed to cover the sidewalls of waveguide structure **14** as shown. The active area of the waveguide **52** is show as dotted line **59** in the cross section of FIG. **4**. An n-type ion implant **60** into a mesa above the n-type modulation doped quantum well interface **26** can be is used to contact the n-type modulation doped quantum well interface **26**. N-type metal **62** contacts to the n-type ion implant **60** to form an n-channel electrode that is electrically coupled to the n-type modulation doped quantum well interface **26**. As is described in detail below, the index of refraction of the waveguide **52** along the coupling region (FIG. **7**) can be varied by application of differential voltage signals between the top electrode **58** and the n-channel electrode **62**. This electrically-controlled change in index of refraction can be used to control the evanescent-wave coupling between the waveguide **52** and the waveguide **44** of the microresonator **12** over the coupling region. Alternatively, the evanescent-wave coupling can be controlled by electrical signals supplied to the thyristor microresonator **12** alone. In this configuration, the top electrode **58**, the n-channel electrode **62**, and the implants **56***a*, **56***b* and **60***b* can be omitted, with the sidewall **54***b* of the waveguide **52** providing lateral confinement in the waveguide **52** over the coupling region.

As seen in FIGS. **1** and **2**, the zig-zag waveguide **52** includes five straight sections coupled by ninety degree bends that are similar in structure to those of the waveguide **44** of the thyristor microresonator **12** as described above. More specifically, each ninety degree bend is defined by a respective forty-five degree facet **64** formed in the sidewalls **54***a*, **54***b* of the waveguide **52**. For efficient coupling in the coupling region of the two waveguides **44**, **52** (FIG. **7**), the widths of the two waveguides **44**, **52** in this coupling region match one another. Note that the width (and/or other cross-sectional parameter) of the zig-zag waveguide **52** can change or taper over its length if required by the design. The zig-zag structure of the waveguide **52** has several advantages, including but not limited to: 1) it allows the width of the waveguide **52** to be greater than the wavelength of the optical mode propagating therein, and thus reduces the dimensional tolerances and associated manufacturing complexities required for smaller wavelengths (such as wavelengths at or near 1 μm); 2) it provides a long interaction length between the microresonator waveguide **22** and the waveguide **52**, which leads to improved coupling efficiency; 3) it allows for effective control over the gap width between the waveguides **52** and **44**—this parameter influences the efficiency of the evanescent-wave coupling between the two waveguides and the Q factor of the microresonator **12**; 4) it eliminates high order modes generated in the gap region since the bend efficiency drops rapidly when the mode order increases, which can improve system performance by reducing noise; and 5) it provides a high packing density in laying out the structures on the substrate.

In one embodiment, the gap region G in the coupling region of the two waveguides **44**, **52** includes implant regions **61***a*,

61*b* of n+ material, which can be formed by localized implantation of a suitable n+ species (such as silicon fluoride ions) into the device structure. The depths of the implant regions **61***a*, **61***b* (which is controlled by the power level during implantation) encompass the n-type and p-type modulation doped quantum well interfaces **22** and **26**, respectively of the device structure as shown in FIG. **4**. The implant regions **61***a*, **61***b* can be formed along with the implant regions **48***a*/**56***a* and **48***b*, **56***b*. The implant regions **61***a*, **61***b* increase the bandgap locally to substantially reduce absorption in the gap region G. This improves the evanescent-wave coupling in coupling region of the two waveguides **44**, **52**. It is also contemplated that the gap region G can be subjected to impurity free vacancy disordering whereby silicon oxide (or other suitable material) covers the gap region G and is then subjected to rapid thermal annealing. The regions outside of the gap region are covered with a dielectric material (or other suitable protective material) during the rapid thermal annealing operation such that there is essentially no effect of impurity free vacancy disordering in these regions. The disordered region increases the bandgap locally to substantially reduce absorption in the gap region G. This can improve the evanescent-wave coupling in the coupling region of the two waveguides **44**, **52**.

It should be noted that for a gap region of small width, the ninety degree bends of the waveguide **52** can be interrupted, and therefore the bend efficiency η_b of the respective bend is reduced as shown in the FIG. **6**. However, the evanescent-wave coupling between the waveguides **52** and **44** generally increases as the width of the gap region G is reduced. Therefore, it is desirable that the design take into account both factors (bend efficiency and evanescent-wave coupling efficiency) in determining the width of the gap region G.

The evanescent-wave coupling between the waveguides **52** and **44** can be modeled mathematically using a model shown in schematic form in FIG. **7**. In this mathematical model, a1 and b1 are the complex amplitudes of the input and output optical signals; a2 and a3 are the complex amplitudes of the optical signals entering the coupling region from the waveguide **52** and from the thyristor microresonator waveguide **44**, respectively; and b2 and b3 are the complex amplitudes of the optical signals leaving the coupling region into the waveguide **52** and into the thyristor microresonator waveguide **44**, respectively. Their relations can be described by the following equations:

$$a_2(t+\delta_1) = \eta_b e^{-j2\pi\nu_0\delta_1} a_1(t), \tag{2}$$

$$\begin{vmatrix} b_2(t+\delta_2) \\ b_3(t+\delta_2) \end{vmatrix} = \begin{vmatrix} t & -j\kappa \\ -j\kappa & t \end{vmatrix} \begin{vmatrix} a_2(t) \\ a_3(t) \end{vmatrix} e^{-j2\pi\nu_0\delta_2}, \tag{3}$$

$$a_3(t+\delta_3) = \eta_m\eta_b^2 e^{-j2\pi\nu_0\delta_3} e^{-\Gamma\alpha v_g\delta_3} b_3(t), \tag{4}$$

where δ_1, δ_2, and δ_3 represent the time for the optical signals to travel between different locations;

η_m is the mode mismatch coefficient accounting for the loss due to the different contact levels;

η_b is the characteristic bend efficiency of the ninety degree corners of the thyristor microresonator waveguide **44**;

ν_0 and v_g are the light frequency and velocity in the semiconductor;

α is the absorption coefficient of the thyristor microresonator waveguide **44**;

Γ is the confinement factor; and

t and κ are coupling coefficients for the coupling region.

The coupling coefficients t and κ can be related to the parameter η_c, which is the loss coefficient due to scattering loss in the gap region G as follows:

$$t^2+\kappa^2=\eta_c^2. \tag{5}$$

Except for the absorption coefficient α, the other parameters used in Eqns. (2) through (5) can be modeled using optical Finite-Difference Time-Domain (FDTD) numerical methods. For an exemplary device with a W of 1 μm, G of 0.25 μm, Offset of 0.2 μm, L1 of 3 μm and L2 of 13 μm, the parameter η_b is 0.995, the parameter η_m is 0.93, the parameter η_c is 0.8356, and the parameter Γ is 0.02. The absorption coefficient α depends upon the amount of charge filling the quantum well(s) of the n-type modulation doped interface **26** of the thyristor microresonator **12**, which can operate to shift the absorption edge of the thyristor microresonator **12** to shorter wavelengths (blue shift). More specifically, a generalized absorption model can be used to represent the absorption coefficient α in terms of the carrier Fermi energy. Then the blue shift of the absorption edge is determined by the charge density of the n-type modulation doped interface **26** in which the Fermi level is controlled by a differential voltage between the anode electrode **30** and the n-channel injector electrode **38**. The absorption model can be based upon a relaxed k-selection rule and Lorentzian weighting function as set forth in Y. Zhang, T. A. Vang, and G. W. Taylor, "Transistor based quantum well optical modulator and its performance in RF links." Proc. SPIE 7817, 12-22 (2010), herein incorporated by reference in its entirety. By using this model, the relation of the absorption coefficient α to photon energy for the thyristor microresonator **12** with different differential bias voltages between the anode electrode **30** and the n-channel injector electrode **38** can be determined as shown in FIG. **8**. The change of absorption coefficient as a function of photon energy can also be determined as shown in FIG. **9**.

The change of the absorption coefficient of the thyristor microresonator **12** changes the real part of the refractive index of the thyristor microresonator **12** as specified by the Kramers-Kronig relations as

$$\Delta n(\omega) = \frac{c}{\pi} P \int \frac{\Delta\alpha(\omega')}{\omega'^2-\omega^2} d\omega' \tag{6}$$

where P is the Cauchy principal integral.

This relation can be used to determine the change in the real part of the refractive index of the thyristor microresonator **12** as a function of photon energy of the thyristor microresonator as shown in FIG. **10**.

Another effect of increased carrier density in the quantum well(s) of the n-type modulation doped interface **26** of the thyristor microresonator **12** is the electro-optic effect caused by the strong electric field at the quantum well-barrier interface. This effect can be represented as:

$$\Delta n_{eo} = \frac{1}{2} r_{41} E_0 n_m^3, \tag{7}$$

where E_o is the quantum well electric field, r_{41} is the linear electro-optical coefficient for <100> GaAs and n_m is the material refractive index.

Therefore, the total change of refractive index in the quantum well(s) of the n-type modulation doped interface **26** of the thyristor microresonator **12** can be expressed as:

$$\Delta n_{qw}=\Delta n_{kk}+\Delta n_{eo}. \quad (8)$$

Evaluation of Δn_{kk} and Δn_{eo} with typical device parameters reveal that for the blue shifted thyristor microresonator **12**, Δn_{kk} is the dominant contributor. The index change Δn_{qw} describes the refractive change in the quantum well alone. The index change of the waveguide **44** of the thyristor microresonator **12** is essentially proportional to Δn_{qw} with a proportionality constant of e_i of approximately 0.2. Hence, the effective refractive index of the waveguide **44** of the thyristor microresonator **12** can be expressed as:

$$n_{eff}=n_m+\Delta n_m=n_m+e_i\Delta n_{qw}. \quad (9)$$

The differential voltage applied between the anode electrode **30** and the n-channel injector electrode **38** of the thyristor microresonator **12** can be used to control the absorption edge of the thyristor microresonator **12** and thus control the absorption coefficient of the thyristor microresonator **12**. According to the Kramers-Kronig relations, the refractive index of the quantum wells of the type modulation doped interface **26** is changed and thus also the effective refractive index of the thyristor microresonator **12**. Basically the effective optical length of the thyristor microresonator **12** is changed and therefore the wavelength spectrum is shifted. In addition, the extinction ratio of the wavelength spectrum has changed. Therefore, for optical input at a fixed wavelength, applied voltage can control the optical coupling between the two waveguides **52**, **44**.

The dependence of the absorption coefficient, refractive index change and transmission of the device as a function of applied bias voltage for an exemplary thyristor microresonator **12** is shown in FIGS. **11**, **12** and **13**, respectively. FIG. **13** shows that for a differential voltage between the anode electrode **30** and the n-channel injector electrode **38** of the exemplary thyristor microresonator **12** near 0.0V, there is reduced evanescent-wave coupling between the waveguides **52** and **44**. This is the pass-thru state of the device where the input optical signal passes through the waveguide **52** with limited optical loss. For a positive differential voltage between the anode electrode **30** and the n-channel injector electrode **38** of the exemplary thyristor microresonator **12** near 1.0V, there is increased evanescent-wave coupling between the waveguides **52** and **44**. This is the coupled state of the device where the input optical signal is transferred from the waveguide **52** to the waveguide **44**. The differential voltage applied to the anode electrode **30** and the n-channel injector electrode **38** can be varied over time between these two levels/states (for example, with a sinusoidal signal whose amplitude varies between these levels) to modulate the input optical signal over time. Note that the extinction ratio of the exemplary thyristor microresonator **12** is about 10.4 dB as is evident from FIG. **13**.

Although changing of the refractive index of the thyristor microresonator **12** can control the transmission of the input optical signal through the coupling region in order to modulate the input optical signal, the transmission curve can be very sensitive to the size of the thyristor microresonator **12**. One solution that addresses this problem is to change the coupling coefficient between the waveguide structure **14** and the thyristor microresonator **12** utilizing electrical control of the channel charge in the waveguide **52** of the waveguide structure **14**. When a positive voltage is applied between the top electrode **58** and the n-channel electrode **62** of the waveguide structure **14**, charge from the top electrode **58** is induced to flow from the top electrode **58** into the adjacent section of the waveguide **52** (in the path of the propagating optical input). This charge induces a refractive index change in the waveguide **52** that reduces the evanescent-wave coupling between the two waveguides **44**, **52** in the coupling region. Thus, by controlling the coupling coefficient independently, the bias voltages of the thyristor microresonator **12** can be fixed and adjusted independently to tune the resonance of the thyristor microresonator **12** to match the input wavelength and to eliminate variability that results from the fabrication and growth procedures. Specifically, the ON state current of the thyristor microresonator **12** controls the charge density in the n-type modulation doped quantum well interface **26** of the epitaxial layer structure of the thyristor microresonator **12**, which controls the effective refractive index in the active area **49** of the waveguide **44** of the thyristor microresonator **12** due to Kramers-Kronig relations. FIG. **14** shows the transmission of the input optical signal through the coupling region of the two waveguides **44**, **52** as a function of bias voltage for this configuration. FIG. **14** shows that for a positive differential voltage between the top electrode **58** and the n-channel electrode **62** of the waveguide structure **14** near 1.0V, there is reduced evanescent-wave coupling between the two waveguides **44**, **53** in the coupling region. This is the pass-thru state of the device where the input optical signal passes through the waveguide **52** with limited optical loss. For a differential voltage between the top electrode **58** and the n-channel electrode **62** of the waveguide structure **14** near 0.0V, there is increased evanescent-wave coupling between the two waveguides **44**, **52** in the coupling region. This is the coupled state of the device where the input optical signal is transferred from the waveguide **52** to the waveguide **44**. The differential voltage applied to the top electrode **58** and the n-channel electrode **62** of the waveguide structure **14** can be varied over time between these two levels/states (for example, with a sinusoidal signal whose amplitude varies between these levels) to modulate the input optical signal over time.

FIG. **15** shows the I-V-P schematic characteristic of an exemplary thyristor microresonator **12**. By setting the DC bias resistance to a corresponding mode specific value, the thyristor microresonator **12** may be biased for a low absorption mode (region A), an optical amplification mode (region B), or a laser operation mode (region C). For optical modulation (FIGS. **16** and **17**), the DC bias resistance is set to a value for the low absorption mode (region A) where the ON state current flow, charge density and absorption loss is minimized. However, for some configurations, the DC bias resistance can be set to a value for the optical amplification mode (region B), which is above the transparency of the quantum wells. Effectively, at the transition into region B, the absorption coefficient α approaches 0. As the bias is increased in region B towards the lasing mode (region C), the function of the optical amplifier is obtained where the absorption coefficient α is effectively negative. The optical amplifier function may compensate for optical losses in a switch fabric or it may be utilized at output port to compensate for the total loss accumulated through any particular path through the switch fabric. The optical amplification mode can also be used to increase the bandwidth of the switch fabric, and/or add additional wavelength channels to the switch fabric.

FIG. **16** shows an exemplary configuration of the thyristor microresonator **12** and optically-coupled waveguide structure **14** for optical modulation. An optical signal source (which could be on-chip or off-chip laser and associated waveguide coupling or other suitable optical element) supplies a continuous-wave optical signal as input to the waveguide **52** of the waveguide structure **14**. The anode electrode **44** of the thyristor microresonator **12** is electrically

coupled to a positive DC voltage (labeled V_{cc}), and the cathode electrode **42** is electrically coupled to ground potential through DC bias resistance **76**. The DC bias resistance **76** can be integrated on-chip (i.e., on the substrate **18**) or off-chip. The DC bias resistance **76** is selected such that the ON state current of the thyristor microresonator **12** is in the low absorbance mode (region A) of FIG. **15**. A DC electrical signal is supplied to the n-channel injector electrode **38** of the thyristor microresonator **12**. The DC electrical signal supplied to the n-channel injector electrode **38** can be selected to tune the resonance wavelength of the thyristor microresonator **12** to match the input wavelength of the input optical signal. This can aid in reducing the variability of the resonance wavelength that results from the fabrication and growth procedures. A time-vary differential signal is supplied to the top electrode **58** and the n-channel electrode **62** of the waveguide structure **14** to modulate the input optical signal over time as described above in detail with respect to FIG. **14**. The modulation of the input optical signal produces a modulated optical signal that propagates from the coupling region of waveguide **52** and is output from the waveguide **52** as shown. The modulated optical signal output from the waveguide **52** can have an optical OOK modulation format (i.e., digital pulsed-mode) or possibly a higher order optical modulation format (such as optical differential phase shift keying format or optical differential quadrature phase shift keying format).

FIG. **17** shows another exemplary configuration of the thyristor microresonator **12** and optically-coupled waveguide structure **14** for optical modulation. An optical signal source (which could be on-chip or off-chip laser and associated waveguide coupling or other suitable optical element) supplies a continuous-wave optical signal as input to the waveguide **52** of the waveguide structure **14**. The anode electrode **44** of the thyristor microresonator **12** is electrically coupled to a positive DC voltage (labeled V_{cc}), and the cathode electrode **42** is electrically coupled to ground potential through DC bias resistance **76**. The DC bias resistance **76** can be integrated on-chip (i.e., on the substrate **18**) or off-chip. The DC bias resistance **76** is selected such that the ON state current of the thyristor microresonator **12** is in the low absorbance mode (region A) of FIG. **15**. A time-vary electrical signal is supplied to the re-channel injector electrode **38** of the thyristor microresonator **12** to modulate the input optical signal over time as described above in detail with respect to FIG. **13**. The modulation of the input optical signal produces a modulated optical signal that propagates from the coupling region of waveguide **52** and is output from the waveguide **52** as shown. The modulated optical signal output from the waveguide **52** can have an optical OOK modulation format (i.e., digital pulsed-mode optical signal) or possibly a higher order optical modulation format (such as optical differential phase shift keying format or optical differential quadrature phase shift keying format).

The optical modulators of FIGS. **16** and **17** are advantageous in that:

- there is relatively low consumption of static power (because the current flow and applied voltage associated with charge control of the quantum well are relatively small);
- higher speed operation is achievable relative to SOI modulator structures (because the problem of charge removal in the intrinsic region of the p-i-n modulator is avoided); and
- the modulator structure is compatible with fabrication of electronic devices (and other optoelectronic devices in the same epitaxial structure.

The thyristor microresonator **12** and optically-coupled waveguide structure **14** can be configured for other optoelectronic functions, including but not limited to a laser (FIG. **18**), an optical detector (FIG. **19**), optical switch (FIG. **20**), and optical switch fabric (FIGS. **21** and **22**).

FIG. **18** shows an exemplary configuration of the thyristor microresonator **12** and optically-coupled waveguide structure **14** for an in-plane laser. The anode electrode **44** of the thyristor microresonator **12** is electrically coupled to a positive DC voltage (labeled V_{cc}), and the cathode electrode **42** is electrically coupled to ground potential through DC bias resistance **78**. The DC bias resistance **78** can be integrated on-chip (i.e., on the substrate **18**) or off-chip. The DC bias resistance **78** is selected such that the ON state current of the thyristor microresonator **12** is in the laser operation mode (region C) of FIG. **15**. A DC electrical signal is supplied to the n-channel injector electrode **38** of the thyristor microresonator **12** such that the thyristor microresonator **12** generates a continuous-wave optical signal that propagates clockwise in the waveguide **44**. The DC electrical signal supplied to the n-channel injector electrode **38** can be selected to tune the resonance wavelength of the thyristor microresonator **12** to match the desired wavelength of the output optical signal. This can aid in reducing variability of the resonance wavelength that results from the fabrication and growth procedures. Concurrent with such operation, a time-vary differential electrical signal (typically an RF signal) is supplied to the top electrode **58** and the n-channel electrode **62** of the waveguide structure **14** to modulate the evanescent-wave coupling between the two waveguides **44**, **52** in the coupling region over time (similar to the modulation described above in detail with respect to FIG. **14**). Such coupling modulation generates a modulated optical signal based upon the continuous-wave optical signal that propagates clockwise in the waveguide **44**. The modulated optical signal propagates from the coupling region of the waveguide **52** and is output from the waveguide **52** as shown. The modulated optical signal output from the waveguide **52** can have an optical OOK modulation format (i.e., digital pulsed-mode optical signal) or possibly a higher order optical modulation format (such as optical differential phase shift keying format or optical differential quadrature phase shift keying format).

Note that the configuration of FIG. **19** transfers the time-varying electrical signal (e.g., RF signal) supplied to the top electrode **58** and the n-channel electrode **62** onto an optical carrier derived from the continuous-wave optical signal that propagates clockwise in the waveguide **44**. This combines the continuous wave laser function and modulation function into the structure of the thyristor microresonator. This is significantly different than the typical prior art where a continuous wave laser (separate from a modulator device) propagates light to the modulator device and an RF signal is applied to the center contact of the modulator device for modulating. Combining the continuous wave laser function and modulation function into the structure of the thyristor microresonator is efficient and also avoids the problem of tuning the resonance wavelength of the modulator to match the continuous wave laser. Moreover, the configuration of FIG. **19** effectively modulates the reflectivity of the resonance cavity of the thyristor microresonator in accordance with the time-varying electrical signal (e.g., RF signal) supplied to the top electrode **58** and the n-channel electrode **62**. This is the operation of a Q switched laser where the electrical signals that drive to the continuous wave laser remain fixed while concurrently supplying electrical signals that modulate an optical property (the reflectivity R) of the resonance cavity of the thyristor microresonator. In this manner, the photon density in the

resonance cavity increases by changing the reflectivity R (and not by changing the electron density as in gain switching). And the reflectivity R can be changed at very high speed (speed limitation of the modulator) as compared to changing the electron density (as in gain switching). Thus, very high speed optical modulation can be supported.

For continuous-wave emission of the laser, a DC differential electrical signal can be supplied to the gate electrode **58** and the n-channel electrode **62** of the waveguide structure **14** (instead of the time-varying signal for the modulated emission). The DC electrical signal controls the device to operate in the coupled state (similar to the coupled state described above in detail with respect to FIG. **14**). In this coupled state, the continuous-wave optical signal that propagates clockwise in the waveguide **44** is transferred to the waveguide **52** (in the coupling region of waveguide **52**) and is output from the waveguide **52** similar to the modulated optical signal shown in FIG. **18**.

FIG. **19** shows an exemplary configuration of the thyristor microresonator **12** and optically-coupled waveguide structure **14** for an optical detector. A modulated optical signal having an optical OOK modulation format (i.e., digital pulsed-mode optical signal) is supplied as input to the waveguide **52** of the waveguide structure **14**. The input optical signal could be supplied from an off-chip source (such as a fiber optic carrier) or an on-chip optical source. The anode electrode **44** of the thyristor microresonator **12** is electrically coupled to a positive DC voltage (labeled V_{cc}), and the cathode electrode **42** is electrically coupled to ground potential through DC bias resistance **80**. The DC bias resistance **80** can be integrated on-chip (i.e., on the substrate **18**) or off-chip. The DC bias resistance **80** is selected such that the ON state current of the thyristor microresonator **12** is in the low absorbance mode (region A) of FIG. **15**. Electrical signals are supplied to the n-channel injector electrode **38** and p-channel injector electrode **40** of the thyristor microresonator **12** for bias purposes. The electrical signal supplied to the n-channel injector electrode **38** includes a DC component that is selected to tune the resonance wavelength of the thyristor microresonator **12** to match the input wavelength of the input optical signal. This can aid in reducing variability of the resonance wavelength that results from the fabrication and growth procedures. A DC differential signal is supplied to the top electrode **58** and the n-channel electrode **62** of the waveguide structure **14**. The DC electrical signal controls the device to operate in the coupled state (similar to the coupled state described above in detail with respect to FIG. **14**). In this coupled state, the input optical signal that propagates down the waveguide **52** is transferred to the waveguide **44** (in the coupling region of the waveguide **52**), where it propagates in a clockwise fashion around the waveguide **44** of the thyristor resonator **12**. The electrical signal supplied to the n-channel injector electrode **38** of the thyristor resonator **12** includes a bias current source, and the electrical signal supplied to the p-channel injector terminal **40** of the thyristor resonator **12** includes a bias current sink. The bias current source and the bias current sink provide bias currents that draw majority carriers from the n-type and p-type modulation doped quantum well interfaces to the respective electrodes (i.e., electrons from the n-type modulation doped quantum well interface to the n-channel injector electrode **38**, and holes from the p-type modulation doped quantum well interface to the p-channel injector **40**). Such bias currents are set such that when the input optical signal is at an ON level, the optical mode propagating in the waveguide **44** has sufficient intensity to produce photocurrent in excess of these bias currents and produces the critical switching charge in either (or both) of the n-type modulation doped quantum well interface and p-type quantum well interface of the thyristor microresonator **12**. At this critical switching charge, the thyristor microresonator **12** will switch to its conducting/ON state. In the ON state, the current through the thyristor microresonator **12** introduces a voltage drop across bias resistance **80**. When the input optical signal is at the OFF level, the optical mode propagating in the waveguide **44** produces minimal photocurrent and the thyristor microresonator **12** switches to its non-conducting/OFF state because the bias currents drain the respective quantum well interfaces of charge, which causes the channel charge to fall below the holding charge QH. In the OFF state, there is minimal current through the thyristor microresonator **12** and thus there is a minimal voltage drop across the bias resistance **80**. In this manner, the electrical signal waveform produced by the differential voltage across the bias resistance **80** represents the ON/OFF levels of the input optical signal. This is the function of the optical detector.

FIG. **20** shows an exemplary configuration of a pair of thyristor microresonators and optically-coupled waveguide structures for an electrically-controlled optical coupler switch. The configuration employs a first thyristor microresonator **12**A optically-coupled to a first waveguide structure **14**B utilizing evanescent-wave coupling as described above with respect to FIG. **7**, and a second thyristor microresonator **12**B optically-coupled to a second waveguide structure **14**B utilizing evanescent-wave coupling as described above with respect to FIG. **7**. All of these structures (first thyristor microresonator **12**A, first waveguide structure **14**A, second thyristor microresonator **12**B, and second waveguide structure **14**B) are integrally formed on the common substrate **18**. The first and second thyristor microresonators **12**A, **12**B include parallel waveguide sections that are optically coupled together via evanescent-wave coupling as described above with respect to FIG. **7**. An optical signal source (which could be an on-chip or off-chip laser and associated waveguide coupling or other suitable optical element) supplies an optical signal as input to the waveguide **52** of the first waveguide structure **14**A. The anode electrodes **44** of the first and second thyristor microresonators **12**A, **12**B are electrically coupled to a positive DC voltage (labeled V_{cc}). A cathode electrode **42** common to both the first and second thyristor microresonators **12**A, **12**B is electrically coupled to ground potential through DC bias resistance **82**. The DC bias resistance **82** can be integrated on-chip (i.e., on the substrate **18**) or off-chip. The DC bias resistance **82** is selected such that the ON state currents of the first and second thyristor microresonators **12**A, **12**B are in the low absorbance mode (region A) of FIG. **15**. A DC electrical signal is supplied to the n-channel injector electrodes **38** of the first and second thyristor microresonators **12**A, **12**B. The DC electrical signal(s) supplied to the n-channel injector electrodes is(are) can be selected to tune the resonance wavelength of the first and second thyristor microresonators **12**A, **12**B to match the input wavelength of the input optical signal. This can aid in reducing the variability of the resonance wavelength that results from the fabrication and growth procedures. Electrical signals (differential voltage signals) are supplied to the top electrode **58** and the n-channel electrode **62** of the first and second waveguide structures **14**A, **14**B to control the optical switching operation of the device.

In a first mode (pass-thru mode), the electrical signals (differential voltage signals) supplied to the top electrode **58** and the n-channel electrode **62** of the first waveguide structure **14**A controls the coupling between the first waveguide structure **14**A and the first thyristor microresonator **12**A to operate in the pass-thru state (similar to the pass-thru state described

above in detail with respect to FIG. **14**). In this pass-thru mode, the input optical signal passes through the waveguide **52** of the first waveguide structure **14**A with limited optical loss.

In a second mode (switched mode), the electrical signal (differential voltage signal) supplied to the top electrode **58** and the n-channel electrode **62** of the first waveguide structure **14**A controls the coupling between the first waveguide structure **14**A and the first thyristor microresonator **12**A to operate in the coupled state (similar to the coupled state described above in detail with respect to FIG. **14**). In this coupled state, the input optical signal that propagates down the waveguide **52** of the first waveguide structure **14**A is transferred via evanescent-wave coupling to the waveguide **44** of the first thyristor microresonator **12**A, where it propagates in a clockwise fashion around the waveguide **44** of the first thyristor resonator **12**A. The optical signal that propagates clockwise around the waveguide **44** of the first thyristor microresonator **12**A is transferred via evanescent-wave coupling as an optical signal that propagates in a counter-clockwise fashion around the waveguide **44** of the second thyristor microresonator **12**B. The electrical signal (differential voltage signal) supplied to the top electrode **58** and the n-channel electrode **62** of the second waveguide structure **14**B controls the coupling between the second waveguide structure **14**B and the second thyristor microresonator **12**B to operate in the coupled state (similar to the coupled state described above in detail with respect to FIG. **14**). This transfers the optical signal that is propagating counter-clockwise around the waveguide **44** of the second thyristor microresonator **12**B to the waveguide **52** of the second waveguide structure **14**B. This optical signal propagates down the waveguide **52** of the second waveguide structure **14**B for output. In this manner, the input optical signal is selectively output from the two waveguide structures **14**A, **14**B based on electrical control. Similar operations can be used to switch in the input optical signal supplied to the second waveguide structure **14**B for output from the second waveguide structure **14**B or the first waveguide structure **14**A. This is the function of the electrically-controlled optical coupler switch.

The optical coupler switch of FIG. **20** can be used as a building block for a monolithic optical switching fabric as shown in the exemplary embodiment of FIG. **21**. This exemplary switch fabric is a 4×4 switching topology employing six of the optical coupler switches of FIG. **20**. In the example shown, the optical coupler switches S_1, S_3, and S_5 are configured in the switched mode while the remainder is configured in the pass-thru mode in order to switch the optical signal from the input port labeled In_1 to the output port labeled Out_4. In another example shown, the optical coupler switch S_1 is configured in the switched-mode while the remainder is configured in the pass-thru mode to switch the optical signal from the input port labeled In_2 to the output port labeled Out_1. In yet another example shown, the optical coupler switch S_3 is configured in the switched-mode while the remainder is off in order to switch the optical signal from the input port labeled In_3 to the output port labeled Out_2. The signal paths are shown by solid and dashed lines through the switch fabric. An advantage of this topology is that there are no waveguide crossings that introduce optical losses that could limit the scalability of the switching fabric. Moreover, the switch fabric can be arranged for a non-blocking architecture. That is, when a certain pathway between an input port and an output port is established, any other pathway may also be established with the remaining input and output ports, provided that each input is routed to a unique output port.

The optical coupler switch of FIG. **20** can also be used as a building block for a monolithic optical switching fabric that employs wavelength division multiplexing capabilities. In such a configuration, one or more optical coupler switches of FIG. **20** can be coupled in a parallel arrangement sharing common input and output waveguides. Each switch in the parallel arrangement would be tuned to a different resonance frequency, allowing inputs with signals on multiple wavelengths to be routed independently while sharing the input and output waveguides. In an exemplary embodiment shown in FIG. **22**, the optical coupler switch pairs S_0/S_0', S_1/S_1', S_2/S_2', S_3/S_3', S_4/S_4', and S_5/S_5' are each configured in a parallel arrangement and tuned to two different resonance frequencies. For a given insertion loss limitation, the switch fabric can be expanded in the wavelength domain to allow for increased aggregate throughput. Similar configurations can be used for an optical add/drop multiplexing function.

The thyristor microresonator offers additional unique advantages for the implementation of the optical switch fabric. One of these advantages is the capability to incorporate a memory function into the switching element. In a large switching fabric (i.e. >50×50), it is difficult from a layout point of view to provide dedicated metal traces to every element. If each element could be switched to the appropriate through or cross state and remain in this state during the data routing cycle, a significant simplification and compaction of the fabric could be realized. This can be accomplished by arranging the thyristor microresonators of the switching fabric to be elements of a memory array. In this configuration, the thyristor microresonators of the switch fabric are adapted to be a memory cell in the manner described below with respective FIGS. **23** to **31**. The data stored in each thyristor-based memory cell corresponds to the required settings for input optical data to be routed to the desired output port. The data is stored in the respective thyristor memory cell during the write cycle where the state of each memory location is determined by electrical inputs to the thyristor device. However as FIG. **15** shows, the writing may also be accomplished with a combination of electrical and optical inputs. This allows the opportunity for the state of the memory to be written with optical injection in the x (waveguide) direction and electrical injection in the y (normal to waveguide) direction. Then the data in the optical label can be used to set the state of the switch. The state of the entire memory (i.e. switching fabric) can be erased using the electrical inputs for all the thyristor memory cells. The thyristor memory cell will retain their data if each element has a dedicated load resistor and this is accomplished by using a vertical resistor construction during the fabrication. Finally, the state of the memory (once written) can be retained in the power down mode (with a power of <1 nW per element) for periods in excess of a few milliseconds. This allows for very low power operation of the switching fabric.

In all of the configurations described herein, the resonance frequency of the thyristor microresonator element can vary based on variations in geometry and refractive index occurring during growth and fabrication. A calibration method can be used to ensure that the resonance frequency of the thyristor microresonator element matches the desired wavelength of the signal that it is intended to process. The thyristor microresonator offers a unique opportunity to perform this calibration which can be explained with the help of FIG. **15**. The choice of resistor determines the ON state current flow through the thyristor and corresponding charge densities in the quantum wells. The charge densities control the effective refractive index of the thyristor waveguide and thus indirectly the resonant frequency of each switch in the fabric. Thus a

calibration procedure may be implemented whereby the load resistor is adjusted and then locked in to an appropriate value according to the desired resonance frequency of the thyristor microresonator in its on-state.

In yet another embodiment of the present invention, the thyristor resonator **12** can be adapted to generate and emit light vertically from an aperture defined in a central region of the device inside the closed loop microresonator waveguide **44**. The aperture can be defined by etching away or otherwise patterning the top anode layer **30** such that light can propagate from (or propagate into) the central region of the device inside the closed loop microresonator waveguide **44**. In this case, the implants **48***a* and **48***b* can be patterned to form under the top anode layer **30** but not under the aperture within the central region of the device. This adaptation can be used for the optical detector configuration to emit an optical signal that corresponds to the ON/OFF levels of the input optical signal. It is also contemplated that optical control signals can be introduced vertically into the aperture defined in the central region of the device. Such optical control signals can control the ON/OFF state of the thyristor resonator **12** and/or change the charge density of the n-type modulation doped quantum well interface of the thyristor resonator **12** for optically controlled modulation and coupling control. In these configurations, the vertical dimension of the thyristor resonator **12** can be tuned to the particular wavelength of an optical mode that is emitted or received vertically from the device. More specifically, the vertical dimension of the thyristor resonator is selected to conform to the following:

$$D = \frac{2\pi m\lambda}{n_{eff}}, \tag{10}$$

where D is the vertical dimension of the thyristor resonator;
m is an integer greater than zero;
λ is the wavelength of the optical mode that is to be emitted from or received by the device; and
n_{eff} is the effective refractive index of the device.

Note that the thyristor microresonator can be configured so that the light is guided around the waveguide **44**, while simultaneously emitting (and detecting) light vertically. Then the operation is available that an input optical signal may enter the microresonator coupling waveguide and switch on the thyristor microresonator so that the vertical operation projects light upwards. This is the operation of an on-chip optical signal launching an off chip vertical optical signal. Likewise the vertically propagating optical signal may enter the aperture of a microresonator on another chip. Then that microresonator may be switched on and launch light into the coupling waveguide on its chip. The combination may provide the basis for chip to chip coupling based on optics. Today, the industry is moving in this direction of creating stacked three-dimensional architectures using electrical vias. This combination can be used to replace such electrical vias with optical connections at much lower cost, higher speed and lower power.

In other aspect of the invention, a thyristor memory cell is provided as shown in FIG. **23**. The thyristor memory cell **100** includes two devices (a thyristor device **111** and a resistive load element **113**) integrally formed on a substrate **115**. The thyristor device **111** includes complementary n-type and p-type modulation doped quantum well interfaces **117**, **119** formed between P+ layer(s) **121** and N+ layer(s) **123**. In the preferred embodiment, the thyristor device **111** is defined by a mesa that includes a refractory anode terminal **125** formed adjacent the highly doped top P+ layer **121**. A cathode terminal **127** is operably coupled to a bottom N+ layer **123**. The potential of the cathode terminal **127** is fixed at ground (or a negative potential). An n-channel injector terminal **129** and a p-channel injector terminal **131** are operably coupled to the n-type and p-type modulation doped quantum well interfaces, respectively. The resistive load element **113** is integrally formed on the anode terminal **125**. In the preferred embodiment, the load element **113** is realized by a phase change material sandwiched between the refractory anode metal **125** and a top refractory electrode. The top refractory electrode (which can be realized from tungsten or other suitable metal) is electrically connected to a word line **133** (which can be realized from copper or other suitable metal). The resistance of the phase change material can be changed between a high resistance phase and a low resistance phase (or vice-versa) in response to electrical signals supplied to the two electrodes that sandwich the phase change material. The phase change material can be a chalcogenide glass material that is capable of changing phase between a high resistance amorphous phase and a low resistance crystalline phase (and vice versa) by Joule heating of the material through application of current to the material. This operation allows the thyristor cell **100** to function as a non-volatile memory cell. It can also function as a static memory cell that does not require periodic refresh, or as a dynamic memory cell that does require periodic refresh as described below.

For optical operations, the thyristor device **111** is formed in a resonant cavity defined by a bottom DBR mirror **135** and top DBR mirror **137**. The bottom DBR mirror **137** is preferably formed by selective oxidation of semiconductor layers that underlie the bottom N+ layer **123** of the thyristor device **111**, and the top DBR mirror **135** is preferably formed by deposition of dielectric materials above the refractory metal anode **125** of the thyristor device **111**. A diffraction grating (not shown) can be used to direct light propagating laterally (in plane light) into a vertical mode confined by the bottom and top DBR mirrors. A current blocking implant **139** can be used to steer current into localized regions of the n-channel quantum well interface **117** of the device **111** in order to increase the current density to induce lasing conditions as desired.

The thyristor device **111** switches from a non-conducting/OFF state (where the current I through the device is substantially zero) to a conducting/ON state (where current I is substantially greater than zero) when:

i) the anode terminal **125** is forward biased (e.g. biased positively) with respect to the cathode terminal **127**; and

ii) the voltage between n-channel injector electrode **129** and the anode electrode **125** is forward biased for a period long enough to produce a charge in the n-type modulation doped quantum well interface **117** that is greater than the critical switching charge QCR, which is that charge that reduces the forward breakdown voltage such that no off state bias point exists.

The voltage between p-channel injector electrode **131** and the cathode electrode **127** can also be configured to produce a charge in the p-type modulation doped quantum well interface **119** that is greater than the critical switching charge QCR, which is that charge that reduces the forward breakdown voltage such that no off state bias point exists.

The critical switching charge QCR is unique to the geometries and doping levels of the device. The thyristor device **111** switches from the conducting/ON state (where the current I is substantially greater than zero) to a non-conducting/OFF state (where current I is substantially zero) when the current I through device falls below the hold current of the device for a sufficient period of time such that the charge in

the n-type modulation doped quantum well interface **117** (or the charge in the p-type modulation doped quantum well interface **119**) decreases below the holding charge QH, which is the critical value of the channel charge which will sustain holding action.

As an optoelectronic component, the thyristor device **111** is multifunctional. If the anode terminal **125** is forward biased (e.g. biased positively) with respect to the cathode terminal **127** and the n-channel injector terminal **129** (and/or the p-channel injector terminal **131**) is biased to produce the critical switching charge QCR in the n-type modulation doped quantum well interface **117** (or in the p-type modulation doped quantum well interface **119**), then the thyristor device **111** will switch to its conducting/ON state. If the current I in the conducting/ON state is above the threshold for lasing, then laser emission will occur. This is the operation of a semiconductor laser. If the thyristor device **111** is in the non-conducting/OFF state and light is admitted into the cavity, then the device **111** can function as an optical detector in the sense that when sufficient electron-hole pairs have been generated to produce the critical switching charge QCR in the n-type modulation doped quantum well interface **117** (or in the p-type modulation doped quantum well interface **119**), the thyristor device **111** will switch to its ON state.

The conducting/ON state and the non-conducting/OFF state of the thyristor device **111** of the memory cell stores "1" and "0" bit values, respectively. In the conducting/ON state of the thyristor device ("1" bit value), current flows through the resistive load element **113** into the anode terminal **125** and through the device, which causes a positive voltage difference between the n-channel injector terminal **129** (bit line) and the cathode terminal **127** (ground or negative potential). In the non-conducting/OFF state of the thyristor device ("0" bit value), current does not flow through the resistance load element **113** into the anode terminal **125** and through the device, thus providing minimal voltage difference between the between the re-channel injector terminal **129** (bit line) and the cathode terminal **127** (ground or negative potential).

For electrical read operations, the voltage signal of the n-channel injector terminal **129** (the bit line) represents the bit value of the cell **100**. For optical read operations, the thyristor device **111** can be configured to emit light in its conducting/ON state (ON current in conducting state greater than the threshold lasing current of the device), and not emit light in its non-conducting/OFF state.

The thyristor device **111** can be programmed electrically into the conducting/ON state ("1" bit value) by applying a forward bias (e.g. biased positively) between the anode terminal **125** and the cathode terminal **127** while forward biasing the n-channel injector electrode **129** with respect the anode electrode **125** for a period long enough to produce a charge in the n-type modulation doped quantum well interface **117** that is greater than the critical switching charge QC. The thyristor device **111** can also be programmed optically into the conducting/ON state ("1" bit value) by applying a forward bias (e.g. biased positively) between the anode terminal **125** and the cathode terminal **127** while supplying an optical pulse of sufficient intensity and/or duration into the resonant cavity of the device to produce a charge in the n-type modulation doped quantum well interface **117** that is greater than the critical switching charge QC. The thyristor device **111** can be programmed electrically into the non-conducting/OFF state ("0" bit value) by applying the appropriate voltage levels at the n-channel injector terminal **129** (bit line) and the p-channel injector terminal **131** (erase line) such that the charge in the n-type modulation doped quantum well interface **117** decreases below the holding charge QH.

For non-volatile write applications, the resistive load element **113** can be programmed into a high resistance state such that thyristor device **111** operates in the non-conducting/OFF state ("0" bit value) in a non-volatile manner by applying suitable voltage levels to the word line **133** and the n-channel injector terminal **129** of the device in order to produce a melting of the phase change material of the resistive load element **113**, which causes a change to an amorphous/highly resistive state. The resistive load element **113** can be programmed into a low resistance state such that thyristor device **111** operates in the conducting/ON state ("1" bit value) in a non-volatile manner by applying suitable voltage levels to the word line **133** and the n-channel injector terminal **129** of the device in order to produce current that recrystallizes the phase change material into its crystalline low resistance state.

The reading, writing and non-volatile programming operations of the thyristor memory cell **100** are summarized in FIG. **24**.

FIG. **25** shows a schematic diagram of an exemplary array of thyristor memory cells **100**. The n-channel injector **129** and the p-channel injector **131** for each row of cells are connected to a bit line **151** and erase line **153**, respectively, for the row. The word line **133** for each column of cells is connected to the top electrode of the load resistors **113** for the cells of the column.

Preferably, the thyristor memory cell **100** of the present invention (and possibly other optoelectronic devices, logic circuits and/or signal processing circuits that are fabricated integral thereto) are realized from the inversion quantum-well channel device structures similar to those described in detail in U.S. Pat. No. 6,031,243; U.S. patent application Ser. No. 09/556,285, filed on Apr. 24, 2000; U.S. patent application Ser. No. 09/798,316, filed on Mar. 2, 2001; International Application No. PCT/US02/06802 filed on Mar. 4, 2002; U.S. patent application Ser. No. 08/949,504, filed on Oct. 14, 1997, U.S. patent application Ser. No. 10/200,967, filed on Jul. 23, 2002; U.S. application Ser. No. 09/710,217, filed on Nov. 10, 2000; U.S. Patent Application No. 60/376,238, filed on Apr. 26, 2002; U.S. patent application Ser. No. 10/323,390, filed on Dec. 19, 2002; U.S. patent application Ser. No. 10/280,892, filed on Oct. 25, 2002; U.S. patent application Ser. No. 10/323,390, filed on Dec. 19, 2002; U.S. patent application Ser. No. 10/323,513, filed on Dec. 19, 2002; U.S. patent application Ser. No. 10/323,389, filed on Dec. 19, 2002; U.S. patent application Ser. No. 10/323,388, filed on Dec. 19, 2002; U.S. patent application Ser. No. 10/340,942, filed on Jan. 13, 2003; all of which are hereby incorporated by reference in their entireties. With these structures, a fabrication sequence is used to make all the devices, including an array of thyristor memory cells and supporting electrical and/or optoelectronic devices on a common substrate. In other words, n type and p type contacts, critical etches, etc. are used to realize all of these devices simultaneously on a common substrate. The essential features of this device structure include 1) an n-type modulation doped interface and a p-type modulation doped quantum well interface, 2) self-aligned n-type and p-type channel contacts formed by ion implantation, 3) n-type metal contacts to the n-type ion implants and the bottom n-type layer structure, and 4) p-type metal contacts to the p-type ion implants and the top p-type layer structure. The active device structures are preferably realized with a material system of group
III-V Materials (Such as a GaAs/AlGaAs).

FIG. **26** shows the IV characteristic of a thyristor memory cell **100** according to the present invention. The thyristor has the non-conducting/OFF and the conducting/ON states to store a '0' and '1' respectively. With the thyristor operated this

way it has the function of a flip flop. Therefore, it is an ideal static RAM (SRAM) cell. The cell has two devices (a thyristor and a load) compared to the flip flop (6T cell). Therefore smaller footprint and higher speed. As described above, the n-channel injector terminal is used to write a '1', and the n-channel injector terminal and the p-channel injector terminal are used to write a '0'. In the preferred embodiment, the operations involve writing a "0" globally (clearing all of the thyristor memory cells), and then writing the "1" values to the appropriate cells of the array one column at a time. Read operations can be performed on the thyristor memory cells as required. During the time between a write and read operation, a forward bias (e.g. biased positively) is applied between the anode terminal and the cathode terminal of the thyristor device, and the latching behavior of the thyristor memory cell stores the bit value of the cell. The resistive load element is a thin film resistor integrated onto the top metal contact of the thyristor device. Therefore the footprint of the memory cell is the crosspoint of an array, i.e. the intersection of two minimum line features. This provides for high density.

In the preferred embodiment, the integrated resistive load **113** is realized from a phase change material as described above. This combines two memory functions within a single cell—one memory function from the load resistor, and another memory function from the latching behavior of the thyristor device. This allows the memory cell **100** to function as a static memory cell (SRAM) as well as a non-volatile memory cell. For normal SRAM operation, the load resistor **113** is programmed into its low resistance state and the thyristor memory cell **100** operates as shown in FIG. **27**. For non-volatile applications, the load resistor **113** can be programmed into the "0" or "1" bit values as described above, and the thyristor memory cell **100** operates as shown in FIG. **28**. In the preferred embodiment, the operations involve writing a "0" globally to the load resistors of the array (clearing all of the thyristor memory cells), and then writing the "1" values to the load resistors **113** of the array one column at a time. Read operations can be performed on the thyristor memory cells **100** as required. During the time between a write and read operation, the supply of bias signals to the thyristor device **111** can be removed, and the no-volatile nature of the resistive load **113** stores the bit value of the cell **100**.

The configurable nature of the thyristor memory cell **100** as a static memory cell or a non-volatile memory cell has many advantages, including:

- The same footprint of memory cell is used.
- For all high speed functions, the SRAM operation is utilized.
- NV operation is only necessary for a sudden loss of power. Therefore there is no point is sacrificing speed to use NV '1's and '0's for all memory operations because the NV operations are somewhat slower than the SRAM's. Instead the NV operation is reserved only for those situations when it is required to protect from power loss.

Therefore the kind of operation envisioned is one where the loss of power is monitored by on chip sense circuits. These circuits can operate with ns speeds and can detect power supply changes on microsecond time scales. Therefore the circuits continuously monitor the power supply. If a loss of power is predicted, then before there is a complete voltage drop, the NV writing mechanism kicks in and the state of the memory is captured. Then when power is resumed, the memory state is rewritten back to the SRAM mode and the operation continues. Thus NV operation is utilized only when required and the only overhead penalties are the power failure detect circuits and the NV write circuits.

The thyristor memory cell **100** can also operate a DRAM cell as shown in FIG. **29**. The states are the same as the SRAM of FIG. **27** but there is an additional state called the 'store' state. Thus, after writing either a '1' or a '0', and during the time that a read operation is not required (these represent substantial periods of time when neither writing nor reading are necessary), the cell **100** is powered down to a low voltage (e.g., approximately 0.6V). The charge in the modulation doped quantum well interfaces **117**, **119** cannot escape by conduction because the components have been reduced drastically. Also recombination is essentially zero. Therefore, if a '1' is stored, i.e. the modulation doped quantum well interfaces **117**, **119** of the thyristor device **111** are filled with charge, then they will remain filled for a long time. Simulations have shown that when the voltage is raised back to the SRAM '1' state after 1 sec, there is still enough charge left in the cell, to restore the ON state. That means the data has not been lost. If the store time exceeds some long time, say 2 seconds, then sufficient charge leaks away that a '0' will be obtained upon increasing the voltage. So a refresh operation is required periodically (e.g., once every sec) as shown in FIG. **30**. The advantage gained is ultra-low power. The speed of read and write is identical to the SRAM. Clearly this DRAM has significant advantages which are:

- High speed operation, similar to SRAM cell.
- Selective operation of the cell as an SRAM cell or DRAM cell can be controlled by simply disabling the refresh cycle and the store voltage.
- The NV backup mode of operation is available here as well.
- Extremely low power operation is possible.
- Extremely high density as shown by the array layout (same as SRAM, NVRAM)
- No complex sense amps are required. The active of the thyristor device **111** is its own sense amp.
- Not limited by stored charge as in conventional DRAM. The thyristor device is an active device which can supply current instead of charge-active read.
- Finally, the DRAM, SRAM and NVRAM, have a photonic capability as well due to the optical writing and reading function capabilities of the device.

This allows a linear array of thyristor memory elements **100** to be coupled to a single waveguide in order to detect and store bits of the optical signal carried by the waveguide. This is a perfect solution for the problem of optical data switching at the front of an optical router. These are photonic buffers. They can hold a frame of data (packet of bits) for several data cycles and then can be controlled to retransmit the data onto the network.

The advantages of the thyristor memory cell **100** of the present invention are summarized in FIG. **31**.

There have been described and illustrated herein several embodiments of optoelectronic thyristor microresonator devices and systems based thereon as well as several embodiments of optoelectronic thyristor memory cell devices and systems based thereon. While particular embodiments of the invention have been described, it is not intended that the invention be limited thereto, as it is intended that the invention be as broad in scope as the art will allow and that the specification be read likewise. Moreover, while particular configurations have been disclosed in reference to particular thyristor microresonator devices and systems based thereon, it will be appreciated that other configurations could be used as well. Particularly, different quantum well active device structures can be used. For example, other active device structure with one or more modulation doped quantum well interfaces (e.g., a single n-type or p-type modulation doped quantum well interface) can be used. It will therefore be appreciated by

those skilled in the art that yet other modifications could be made to the provided invention without deviating from its spirit and scope as claimed.

It is the express intention of the applicant not to invoke 35 U.S.C. §112, paragraph 6 for any limitations of any of the claims herein, except for those in which the claim expressly uses the word 'means' together with an associated function.

What is claimed is:

1. A semiconductor device comprising:

an optical resonator for processing light at a predetermined wavelength, the optical resonator including a closed loop waveguide and a central region surrounded by the closed loop waveguide; and

a waveguide structure spaced from the closed loop waveguide of the optical resonator to provide for evanescent-wave optical coupling therebetween;

wherein both the optical resonator and the waveguide structure are formed in an epitaxial layer structure deposited on a substrate, the epitaxial layer structure including at least one modulation doped quantum well interface; and

wherein the central region of the optical resonator includes a first electrode with at least one ion implant region formed under the first electrode and extending through the at least one modulation doped quantum well interface of the epitaxial layer structure adjacent the closed loop waveguide, wherein the at least one ion implant region provides for lateral confinement of light within the closed loop waveguide and for funneling of current from the first electrode away from the central region and through the closed loop waveguide of the optical resonator.

2. A semiconductor device according to claim **1**, wherein:

the optical resonator further includes a second electrode that cooperates with the first electrode to provide for DC current that flows through the closed loop waveguide, and the at least one ion implant region provides for funneling of said DC current away from the central region and through the closed loop waveguide of the optical resonator.

3. A semiconductor device according to claim **2**, wherein:

charge density in the at least one modulation doped quantum well interface of the epitaxial layer structure of the closed loop waveguide controls the refractive index of the closed loop waveguide, wherein said DC current that flows through the closed loop waveguide of the optical resonator affects the charge density in the at least one modulation doped quantum well interface of the epitaxial layer structure of the closed loop waveguide and the refractive index of the closed loop waveguide.

4. A semiconductor device according to claim **2**, further comprising:

a third electrode electrically coupled to the modulation doped quantum well interface of the epitaxial layer structure of the closed loop waveguide.

5. A semiconductor device according to claim **4**, wherein:

a time-varying electrical signal is supplied to the third electrode to vary charge density in the at least one modulation doped quantum well interface of the epitaxial layer structure of the closed loop waveguide in order to change the refractive index of the closed loop waveguide and modulate the evanescent-wave coupling between the closed loop waveguide and the waveguide structure.

6. A semiconductor device according to claim **4**, wherein:

a DC electrical signal is supplied to the third electrode to control charge density in the at least one modulation doped quantum well interface of the epitaxial layer structure of the closed loop waveguide in order to control the refractive index of the closed loop waveguide.

7. A semiconductor device according to claim **1**, wherein:

for at least one straight section of the waveguide structure that is optically coupled to one section of the closed loop waveguide, at least one additional ion implant region is formed such that it extends through the at least one modulation doped quantum well interface of the epitaxial layer structure of the waveguide structure, wherein the at least one additional ion implant region provides for lateral confinement of light with the waveguide structure.

8. A semiconductor device according to claim **1**, wherein:

the waveguide structure includes fourth and fifth electrodes that provide for current flow through the at least one modulation doped quantum well interface of the epitaxial layer structure of the waveguide structure.

9. A semiconductor device according to claim **8**, wherein:

a time-varying electrical signal is supplied to the fourth and fifth electrodes to vary charge density in the at least one modulation doped quantum well interface of the epitaxial layer structure of the waveguide structure in order to change the refractive index of the waveguide structure and modulate the evanescent-wave coupling between the closed loop waveguide and the waveguide structure.

10. A semiconductor device according to claim **1**, wherein:

the closed loop waveguide is rectangular in nature with four straight sections coupled by ninety degree bends.

11. A semiconductor device according to claim **10**, wherein:

each ninety degree bend includes an outside facet and a cut inside corner that extends parallel to the outside facet, wherein the outside facet is defined a sidewall in the epitaxial layer structure and the cut inside corner is defined by the profile of the at least one ion implant.

12. A semiconductor device according to claim **10**, wherein:

the waveguide structure has a zig-zag path with five straight sections coupled by ninety degree bends.

13. A semiconductor device according to claim **1**, further comprising:

a plurality of distributed bragg reflector (DBR) mirror layers formed on the substrate below the at least one modulation doped quantum well interface of the epitaxial layer structure of the optical resonator and the waveguide structure.

14. A semiconductor device according to claim **13**, further comprising:

a plurality of dielectric mirror layers formed on the substrate above the epitaxial layer structure of the optical resonator and the waveguide structure.

15. A semiconductor device according to claim **1**, wherein:

said epitaxial layer structure includes an N+ type doped layer, a first plurality of layers that define a p-type modulation doped quantum well interface formed above said N+ type doped layer, a second plurality of layers that define an n-type modulation doped quantum well interface formed above said first plurality of layers, and a P+ type doped layer spaced from said second plurality of layers.

16. A semiconductor device according to claim **15**, wherein the optical resonator is formed by:

a top p-type metal layer which contacts the P+ type doped layer; and

N+ type ion implanted regions which contact the n-type modulation doped quantum well interface;

an n-type metal layer that contacts the N+ type ion implanted regions; and

a bottom n-type metal layer that contacts the N+ type doped layer;

wherein the optical resonator realizes a thyristor in which said top p-type metal layer is the first (anode) electrode of the thyristor, said bottom n-type metal layer is the cathode electrode of the thyristor, and the n-type metal layer that contacts the n-type modulation doped quantum well interface is an injector terminal of the thyristor.

17. A semiconductor device according to claim **16**, wherein:

the anode and cathode electrodes provide for DC current that flows through the closed loop waveguide, and the at least one ion implant region provides for funneling of said DC current away from the central region and through the closed loop waveguide of the optical resonator.

18. A semiconductor device according to claim **17**, wherein:

said DC current that flows through the closed loop waveguide of the optical resonator affects charge density in the at least one modulation doped quantum well interface of the epitaxial layer structure of the closed loop waveguide and the refractive index of the closed loop waveguide.

19. A semiconductor device according to claim **16**, wherein:

a time-varying electrical signal is supplied to the injector terminal to vary charge density in the n-type modulation doped quantum well interface of the epitaxial layer structure of the closed loop waveguide in order to change the refractive index of the closed loop waveguide and modulate the evanescent-wave coupling between the closed loop waveguide and the waveguide structure.

20. A semiconductor device according to claim **16**, wherein:

a DC electrical signal is supplied to the injector terminal to control charge density in the n-type modulation doped quantum well interface of the epitaxial layer structure of the closed loop waveguide in order to control the refractive index of the closed loop waveguide.

21. A semiconductor device according to claim **20**, wherein:

the waveguide structure includes fourth and fifth electrodes that provide for current flow through an n-type modulation doped quantum well interface of the epitaxial layer structure of the waveguide structure; and

a time-varying electrical signal is supplied to the fourth and fifth electrodes to vary charge density in the n-type modulation doped quantum well interface of the epitaxial layer structure of the waveguide structure in order to change the refractive index of the waveguide structure and modulate the evanescent-wave coupling between the closed loop waveguide and the waveguide structure.

22. A semiconductor device according to claim **1**, further comprising:

at least one additional ion implant region that extends through the at least one modulation doped quantum well interface of the epitaxial layer structure for a gap region between the closed loop waveguide and the waveguide structure.

23. A semiconductor device according to claim **1**, wherein:

the optical resonator is configured to operate as an optical modulator that modulates a continuous-wave optical signal supplied to the input of the waveguide structure in order to produce a modulated optical signal at the output of the waveguide structure.

24. A semiconductor device according to claim **1**, wherein:

the optical resonator is configured to operate an in-plane laser that produces an optical signal that is transferred to the waveguide structure and emitted from the output of the waveguide structure.

25. A semiconductor device according to claim **24**, wherein:

electrical signals are applied to the device to modulate the evanescent-wave coupling between the closed loop waveguide and the waveguide structure in order to modulate the optical signal produced at the output of the waveguide structure.

26. A semiconductor device according to claim **1**, wherein:

the optical resonator is configured as a detector that produces an output signal corresponding to ON/OFF levels of an input optical signal supplied to the input of the waveguide structure.

27. A semiconductor device according to claim **1**, wherein:

the optical resonator is configured as a vertical cavity surface emitting laser (VCSEL) whereby current flow in the on state exceeds a laser threshold for producing light emission from an optical aperture.

28. A semiconductor device according to claim **1**, wherein:

the optical resonator and the waveguide structure comprise a first device pair;

an additional optical resonator and an additional waveguide structure formed on the substrate comprise a second device pair;

the optical resonators of the first and second device pairs are optically coupled to one another by evanescent-wave coupling; and

the device is configured as an optical switch for selectively transferring an input optical signal supplied to the input of one of the first and second waveguide structures to the output of one of the first and second waveguide structures.

29. An optical switch fabric comprising:

an array of the semiconductor devices of claim **28** integrally formed on the substrate.

30. An optical switch fabric of claim **29**, wherein:

the optical resonators of the array are adapted to switch different wavelength signals in order to support switching of wavelength division multiplexed optical signals input to the optical switch fabric.

31. A semiconductor device according to claim **1**, wherein:

length of the closed loop waveguide corresponds to the particular wavelength of light.

32. A semiconductor device according to claim **1**, wherein:

the at least one modulation doped quantum well interface of the epitaxial layer structure includes an n-type modulation doped quantum well interface offset vertically from a p-type modulation doped quantum well interface; and

the at least one ion implant formed under the first electrode includes a first ion implant region offset vertically from a second ion implant region, where the first ion implant region extends through the n-type modulation doped quantum well interface of the epitaxial layer structure adjacent the closed loop waveguide, and wherein the second ion implant region extends through the p-type modulation doped quantum well interface of the epitaxial layer structure adjacent the closed loop waveguide.

* * * * *